

Spherical Domain Wall formed by Field Dynamics of Hawking Radiation and Structure Near Horizon

Yukinori Nagatani*

*Department of Particle Physics,
The Weizmann Institute of Science, Rehovot 76100, Israel*

Abstract

The Hawking radiation in the vacuum of the spontaneous symmetry breaking in the gauge-Higgs-Yukawa theory is investigated by a general relativistic formulation of the ballistic model. The restoration of the symmetry on the horizon and the formation of the spherical domain wall around the black hole are shown even if the Hawking temperature is lower than the critical temperature of the phase transition in the gauge-Higgs-Yukawa theory. When the Hawking temperature is much lower than the critical temperature, the domain wall closely near the horizon is formed. The wall is formed by the field dynamics rather than the thermal phase transition.

*e-mail: yukinori.nagatani@weizmann.ac.il

1 INTRODUCTION

One of the most interesting in the quantum field theory with the general relativity is the thermal radiation from black holes, which is known as the Hawking radiation [1, 2]. The temperature and the intensity of the radiation from the Schwarzschild black hole increase explosively at the final stage of the evaporation because the black hole loses its mass by the radiation and its temperature is inversely proportional to the mass [2]. Therefore the particle physics and the field dynamics including phase transitions around the black hole are especially interesting. Several authors discussed that the heating-up by the Hawking radiation can thermalize the neighborhood of the black hole and the *thermal* phase transition around the black hole can arise. Cline considered the QCD phase transition around the black hole whose Hawking temperature is greater than the critical temperature of the quark-gluon-plasma (QGP) transition [3]. He pointed out that some of the gamma ray bursts can be explained by the radiation from the QGP fireballs produced by the Hawking radiation from the primordial black holes. We showed the thermal electroweak (EW) phase transition around the black hole and the formation of the spherical domain wall which separates the symmetric-phase-region from the broken-phase background [4, 5]. We discussed several mechanisms of the baryon-number-production by the spherical domain wall around a black hole and proposed the cosmological baryogenesis scenario by the primordial black holes [4, 5, 6].

The thermal phase transition on some local volume requires the local thermal equilibrium which is confirmed by the enough interaction rate in the considered volume. The mean free paths of the radiated particles are much longer than the Schwarzschild radius. If the thermal phase transition is caused by heating-up by the Hawking radiation, the radius of the wall should be much larger than the Schwarzschild radius. Hence the formation of the wall by the thermal phase transition needs much higher Hawking-temperature than the critical temperature of the transition [4, 5]. Here, it is natural to ask if the Hawking radiation whose temperature is similar to the critical temperature of the transition influences the Higgs vacuum-expectation-value (vev) around the black hole. In our previous work [8, 9], we considered the Hawking radiation with such a temperature in the gauge-Higgs-Yukawa theory, e.g., the EW theory or the Grand Unified Theory (GUT). We proposed *the ballistic model* as an effective description of the system. By using the ballistic model, the formation of the wall-structure of the Higgs vev was shown when the Hawking temperature is equal to or greater than the energy scale of the gauge-Higgs-Yukawa theory. The wall-structure is formed by the field dynamics rather than the thermal phase transition.

The ballistic model is described by both the action for the Higgs scalar field and that for the relativistic point particles as the Hawking-radiated particles from the black hole. The ballistic description of the radiated particle is valid because the mean free paths determined by gauge

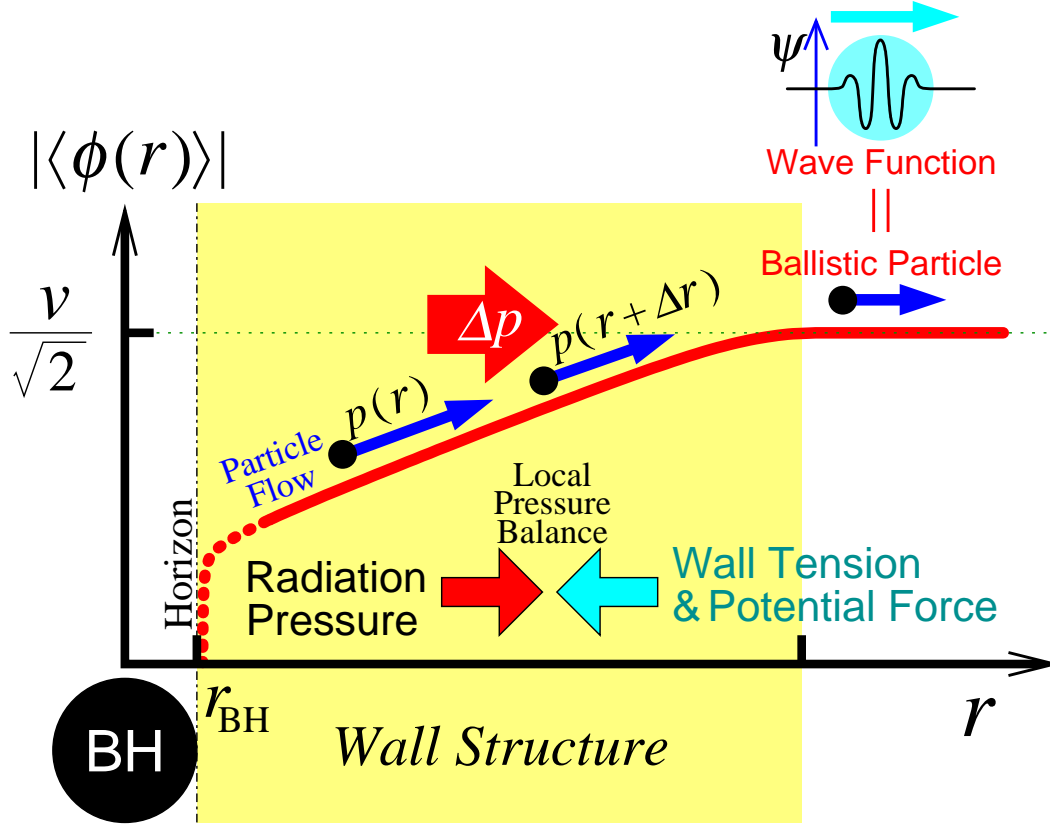


Figure 1: The balance of pressures — our basic idea for the wall-formation in the ballistic model. The parameter r is the distance from the center of the black hole and $|\langle \phi(r) \rangle|$ means the absolute value of the Higgs vev. Once a wall-structure of Higgs vev (thick curve) is formed, mass of the particle is depending on the distance r . A part of the momentum of the Hawking-radiated particle $\Delta p = p(r) - p(r + \Delta r)$ is transferred to the wall-structure because the momentum is depending on the distance r in the wall-structure: $p(r) = \sqrt{E^2 - m(r)^2}$. The transferred momentum causes a radiation-pressure acting on the wall. A local balance among the radiation-pressure, the wall-tension and the potential-force can stabilize the wall-structure. The dotted thick curve means the wall-structure near the horizon. The radiation pressure near the horizon is enhanced due to a general relativistic effect and forms the wall-structure near the horizon.

interactions are much longer than the Schwarzschild radius [4, 5] and the mean wavelength of the radiated particles approximately given by the Schwarzschild radius is shorter than the length-scale of the wall-structure [8, 7]. The basic idea of the wall formation in the ballistic model is schematically shown in Figure 1. When once a radius-dependent Higgs-vev-structure $|\langle\phi(r)\rangle|$, namely the wall-structure, has been formed, the Hawking-radiated particles run rush up the slope on the wall-structure and they push the wall-structure outside. Therefore there arises a pressure, named the Hawking-radiation-pressure, which is acting on the spherical wall-structure to expand its radius. On the other hand the wall-structure also feels its wall-tension and the Higgs-potential-force, which are acting on the wall-structure to shrink its radius. The balance among these pressures keeps the wall-structure stationary.

In the previous work [8], the black hole is assumed as a simple source of the particles with thermal spectrum and general relativistic (GR) effects are omitted. In this paper we fully consider the GR effects in the ballistic model and show the formation of the wall-structure if the Hawking temperature is not only greater than the energy-scale of the gauge-Higgs-Yukawa theory but also smaller than the energy-scale. We assume that (i) the motion of the particles radiated from the horizon obeys the geodesic on the Schwarzschild space-time and (ii) the observer at the infinite distance detects the disk-image with uniform intensity as an image of the radiated particles. By constructing the general relativistic formulation of the ballistic model we derive the effective Higgs potential including full GR effects, which determines the Higgs vev structure around the black hole. The effective potential is depending on the differential particle-density-distribution $dE \times \mathcal{N}(E, r)$ of both the particle-position r and the particle-energy E . The analysis of the particle-trajectories radiated from the horizon gives us the density-distribution. The density-distribution $dE \times \mathcal{N}(E, r)$ is depending on the differential particle-flux $dE \times d\omega \sin \omega \times f(E, \omega)$ on the horizon because the initial conditions for the particles are given by the flux $f(E, \omega)$ on the horizon. The parameter ω is a zenith-angle of the particle-radiation on the horizon. The elevation-angle of the radiation becomes $(\pi/2 - \omega)$. The particle-flux for high elevation-angles is derived by the two assumptions above-mentioned because particles radiated with the high elevation-angle can be detected by the observer and their trajectories can be traced. On the other hand, the particle-flux for low elevation-angles cannot be determined by the assumptions because the particles radiated with a low elevation-angle return into the horizon and are not detected by the observer. By the analytic continuation of the particle-flux from the high elevation-angle to the low elevation-angle, we can obtain the particle flux for all angle. Then we can derive the effective potential and the effective differential equation for the Higgs scalar vev around the black hole. The suitable boundary conditions for the differential equation are as follows; (i) the Higgs vev $\langle\phi(r)\rangle$ approaches the ordinary Higgs vev $\langle\phi\rangle = v/\sqrt{2}$ which minimizes the bare Higgs potential $V(\phi)$ when the distance from the black hole approaches infinity $r \rightarrow \infty$ and (ii)

the Higgs vev should be finite on the horizon. The field equation is numerically solved with the boundary conditions and the wall-structure of the Higgs vev around the black hole is obtained.

Our resultant wall-structure has two interesting properties as follows. The Higgs wall structure is formed even if the Hawking temperature is much smaller than the energy scale of the gauge-Higgs-Yukawa theory. When we consider such a low temperature black hole, there arises a wall-structure closely near the horizon. The Higgs vev on the horizon becomes zero, namely, the symmetry broken-down spontaneously by the Higgs potential is restored on the horizon. These properties are not found in the previous work [8] and are essentially caused by the GR effects on the Hawking-radiated particles.

In Section 2 the general relativistic formulation of the ballistic model is given and the general form of the effective Higgs potential V_{eff} is obtained. The effective potential V_{eff} is depending on the differential density-distribution $dE \times \mathcal{N}(E, r)$ of the radiated particle. In Section 3 various patterns of the particle-trajectories are analyzed and the form of the density-distribution $dE \times \mathcal{N}(E, r)$ is obtained as a functional of the differential flux on the horizon $dE \times d\omega \sin \omega \times f(E, \omega)$. In Section 4 the flux $dE \times d\omega \sin \omega \times f(E, \omega)$ is discussed. In Section 5 the concrete form of the density-distribution $dE \times \mathcal{N}(E, r)$ is obtained by using the results of Section 3 and Section 4. In Section 6 the differential equation for the Higgs vev and the boundary conditions are discussed and the formation of the wall-structure is shown. In section 7 we provide a conclusion and discussions. In Appendix A another argument of the flux on the horizon $dE \times d\omega \sin \omega \times f(E, \omega)$ is given. In Appendix B the energy-density of the Hawking-radiated particles around the black hole is calculated. In Appendix C analytic solutions near the horizon are discussed.

2 Ballistic Model with General Relativity

The ballistic model is an effective theory for computing the structure of the Higgs vacuum expectation value (vev) around a black hole radiating particles in the vacuum of the gauge-Higgs-Yukawa theory [8]. The Hawking-radiated particle can be regard as ballistic because the radiated particle has a longer mean free path and has a shorter wavelength than the radius of the wall-structure which we will discuss later. The ballistic particle is identified with a relativistic point particle with interactions. In the ballistic model the Higgs scalar field is separated into the Higgs vev and the ballistic Higgs particles [8]. The Higgs vev is depending on the position but is not depending on the time. The ballistic Higgs particle describes the Higgs propagating mode in the background of the Higgs vev. The ballistic model consists of the time-independent Higgs scalar vev $\phi(x)$ and a set of the trajectories of the ballistic particles $\{y_i^\mu(s)\}$, where i denotes an index of each particle and s is a parameter of

the trajectory. The set of the ballistic particles $\{y_i^\mu(s)\}$ contains all radiated particles around the black hole, which also includes the ballistic Higgs particles. The fundamental action for the ballistic model is given by a combination of an action for the Higgs scalar vev $\phi(x)$ with a Higgs potential $V(\phi)$ and an action for the trajectories $\{y_i^\mu(s)\}$ of relativistic point particles as the ballistic particles:

$$S[\phi, y] = \int d^4x \sqrt{g} \left[g^{\mu\nu} \partial_\mu \phi \partial_\nu \phi - V(\phi) \right] - \sum_i \int ds Y_i |\phi(y_i)| \sqrt{g_{\mu\nu} \dot{y}_i^\mu \dot{y}_i^\nu}, \quad (1)$$

where we have defined $\dot{y}_i^\mu := dy_i^\mu/ds$ and the summation is performed over all ballistic particles. The background space-time is given by the Schwarzschild metric:

$$ds^2 = +F(r)dt^2 - F^{-1}(r)dr^2 - r^2d\theta^2 - r^2 \sin^2 \theta d\varphi^2, \quad (2)$$

with the Schwarzschild factor:

$$F(r) := 1 - \frac{r_{\text{BH}}}{r}. \quad (3)$$

The bare Higgs potential in the action is given by the double-well form:

$$V(\phi) = -\frac{1}{2}\mu^2\phi^2 + \frac{1}{2}v^2\phi^4, \quad (4)$$

which has a minimum at $|\phi| = v/\sqrt{2}$ and the constant $\mu^2 > 0$ is the Higgs mass, therefore, the Higgs vev without the Hawking radiation is given by $|\langle \phi \rangle| = v/\sqrt{2}$. We have defined an extended-Yukawa-coupling-constant Y_i for the point particle i . The mass of the particle i is proportional to the Higgs vev and is given by

$$m_i = Y_i |\langle \phi \rangle|, \quad (5)$$

where the mass relation in the gauge-Higgs-Yukawa theory is reproduced. Especially mass of the particle i in the vacuum is given by $m_i = Y_i |\langle \phi \rangle| = Y_i v/\sqrt{2}$. The ballistic Higgs particles does not obey the relation (5), however, by choosing

$$Y_{\text{Higgs}} = \sqrt{3} \frac{\mu}{v} \quad (6)$$

as the extended-Yukawa-coupling-constant for the ballistic Higgs particles, the action (1) results in the correct effective potential (see Appendix in [8]). The formulation presented above is a simple general relativistic extension of the original ballistic model in the previous work [8].

By a gauge fixing $ds = dt = y_i^t$ and employing the Schwarzschild coordinate (t, r, θ, φ) , the action becomes

$$\begin{aligned} S[\phi, y] &= \int dt dr d\theta d\varphi r^2 \sin \theta \\ &\times \left[F^{-1} \dot{\phi}^2 - F (\partial_r \phi)^2 - r^{-2} (\partial_\theta \phi)^2 - r^{-2} \sin^{-2} \theta (\partial_\varphi \phi)^2 - V(\phi) \right. \\ &\left. - \sum_i Y_i |\phi(t, r, \theta, \varphi)| \frac{1}{\gamma_i} \frac{\delta(r - y^r) \delta(\theta - y^\theta) \delta(\varphi - y^\varphi)}{r^2 \sin \theta} \right], \quad (7) \end{aligned}$$

where we have defined a general relativistic gamma factor for particle y_i as

$$\gamma_i = \left[F - F^{-1}(\dot{y}_i^r)^2 - r^2(\dot{y}_i^\theta) - r^2 \sin \theta (\dot{y}_i^\varphi)^2 \right]^{-1/2}. \quad (8)$$

We assume spherical symmetry of the Higgs vev $\phi(r)$ due to the spherical symmetry of the metric and the Hawking radiation. The equation of motion for the Higgs vev with the condition $\partial_t \phi = 0$ becomes

$$\Delta \phi = \frac{1}{2} \frac{\partial V}{\partial \phi} + \frac{1}{2} \frac{\partial |\phi|}{\partial \phi} \sum_i Y_i \frac{1}{\gamma_i} \frac{\delta(r - y_i^r) \delta(\theta - y_i^\theta) \delta(\varphi - y_i^\varphi)}{r^2 \sin \theta}, \quad (9)$$

where we have defined a Laplacian with spherical symmetry

$$\Delta \phi := + \frac{1}{r^2} \partial_r (r^2 F \partial_r \phi). \quad (10)$$

Because the metric and the Higgs vev as a background of the ballistic particles have an invariance of the time-evolution and have spherical symmetry, there are two constants of motion for each ballistic particle, namely, the energy E_i and the angular momentum L_i . By using spherical symmetry we select the coordinate system individually for each particle trajectory to keep $y_i^\theta = 0$. The motion of each particle is described on each plane (y_i^r, y_i^φ) . By using constants of the motion, the equation of motion for the ballistic particles becomes

$$E_i = Y_i |\phi(y_i^r)| \gamma_i(t) F(y_i^r), \quad (11)$$

$$L_i = Y_i |\phi(y_i^r)| \gamma_i(t) r^2 \dot{y}_i^\varphi. \quad (12)$$

By substituting (11) into (9) and using property of the Dirac delta function, we obtain

$$\Delta \phi = \frac{1}{2} \frac{\partial V}{\partial \phi} + \frac{1}{2} \frac{\partial |\phi|}{\partial \phi} \sum_i Y_i^2 F(r) \frac{|\phi(r)|}{E_i} \frac{\delta(r - y_i^r) \delta(\theta - y_i^\theta) \delta(\varphi - y_i^\varphi)}{r^2 \sin \theta}. \quad (13)$$

We define the effective potential as

$$V_{\text{eff}}(\phi, y) := V(\phi) + \frac{1}{2} \phi^2 F(r) \sum_i Y_i^2 \frac{1}{E_i} \frac{\delta(r - y_i^r) \delta(\theta - y_i^\theta) \delta(\varphi - y_i^\varphi)}{r^2 \sin \theta}, \quad (14)$$

then the equation of motion for the Higgs vev becomes

$$\Delta \phi = \frac{1}{2} \frac{\partial V_{\text{eff}}}{\partial \phi}. \quad (15)$$

Instead of considering the effect of each ballistic particle, we will statistically treat the group of the particle of the same kind. We adopt a differential distribution of particle-number-density $dE \times \mathcal{N}_f(E, r)$ for particle species f with energy E at the position r . The density-distribution should have the spherical symmetry because of the absence of a special direction of the Hawking radiation. The effective potential (14) becomes

$$V_{\text{eff}}(\phi, r) = V(\phi) + \frac{1}{2} \phi^2 F(r) \sum_f Y_f^2 \int \frac{dE}{E} \mathcal{N}_f(E, r), \quad (16)$$

where the summation in the effective potential (16) is performed over all particle-species $\{f\}$ in the gauge-Higgs-Yukawa theory and Y_f is the extended-Yukawa-coupling-constant for a particle-species f . We rewrite the effective potential (16) as

$$V_{\text{eff}}(\phi, r; \mathcal{N}) = +\frac{1}{2} \mu_{\text{eff}}^2(r; \mathcal{N}) \phi^2 + \frac{1}{2} \frac{\mu^2}{v^2} \phi^4, \quad (17)$$

where we have defined the effective Higgs mass as

$$\mu_{\text{eff}}^2(r; \mathcal{N}) = -\mu^2 + F(r) \sum_f Y_f^2 \int \frac{dE}{E} \mathcal{N}_f(E, r). \quad (18)$$

The effective Higgs mass (18) which governs the effective potential (17) is a functional of the density-distribution $\mathcal{N}_f(E, r)$. Therefore we have found the Higgs vev structure around the black hole is determined by the density-distribution of the Hawking-radiated particles.

3 Density of the Ballistic Particles I

In this section we calculate the density-distribution $\mathcal{N}_f(E, r)$ of the ballistic particles radiated from the black hole. To determine the density-distribution we assume as follows:

- (i) The particles are radiated from the horizon and obey the equations of the motion in (11) and (12) on the Schwarzschild space-time (2).

The configuration of our setup is schematically shown in Figure 2. A part of radiated particles reach infinite distance. The initial condition for the particle is given by the position (θ, φ) where the particle radiate on the horizon, the radiation-angle (ω, ψ) on the position and the energy E which is defined in (11). ω is a zenith-angle defined for $0 \leq \omega < \pi/2$ and ψ is a azimuthal angle defined for $0 \leq \psi < 2\pi$. The zenith-angle ω is defined by the angle which the trajectory of the particle and the perpendicular of the horizon make on the horizon. The zenith-angle ω is defined on the Schwarzschild coordinate. The elevation-angle of the radiation becomes $(\pi/2 - \omega)$.

We put the differential number-flux of the Hawking-radiated particles per an unit area on the horizon with the Schwarzschild coordinate

$$d\mathcal{F}_f = f_f(E, \omega) \times dE \times d\omega \sin \omega d\psi \quad (19)$$

which depends on the energy E of the particle and on the zenith-angle ω of the radiation. The flux (19) is independent of the position (θ, ϕ) and of the azimuthal angle ψ due to the spherical symmetry. The form of the particle-trajectory is determined by the particle-energy E and zenith-angle ω of the radiation as the initial conditions, and is also determined by the mass of the particle, i.e., the product of the extended-Yukawa-constant Y_f and the Higgs vev $|\phi(r)|$ as the back ground. Then the density-distribution $\mathcal{N}_f(E, r)$ is obtained by the analysis of the particle-trajectories and is depending on the flux $f_f(E, \omega)$.

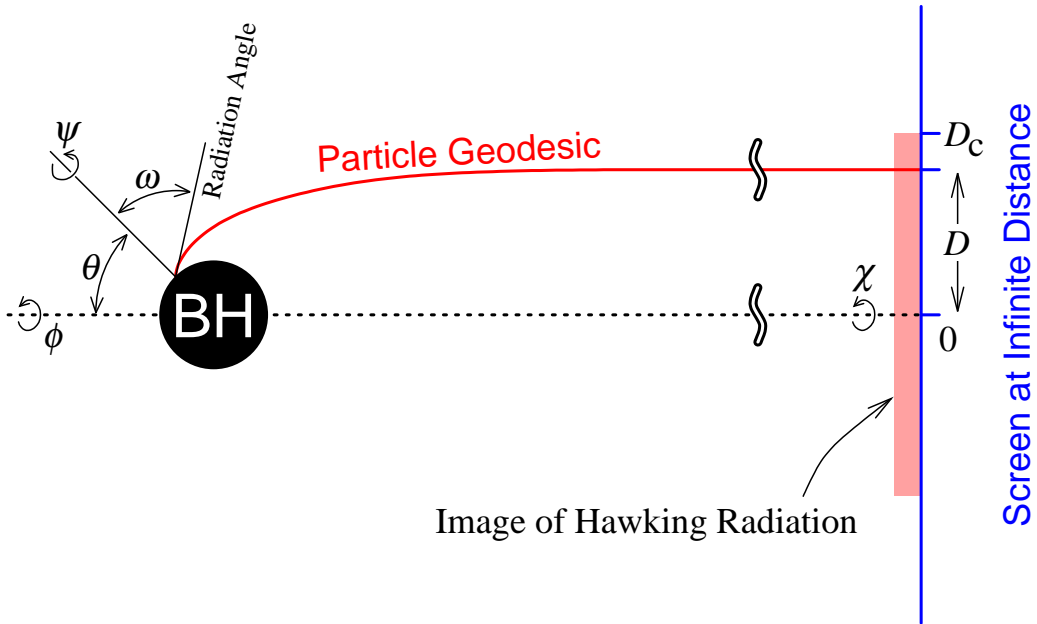


Figure 2: The configuration of our setup — the coordinate (θ, ϕ) of the horizon, the radiation-angle (ω, ψ) on the horizon and the screen at the infinite distance. ω is the zenith-angle and ψ is the azimuthal-angle of the radiation on the horizon. The elevation-angle of the radiation becomes $(\pi/2 - \omega)$. The screen is parameterized by the polar coordinate (D, χ) , where D is the distance from the center of the screen and χ is the angle. D is identified as the impact-parameter of the particle-geodesic. The observer at the infinite distance finds an image of a disk as a detection of the Hawking radiation. D_c is the radius of the disk-image, which is depending on the ratio of the particle-energy E to the particle-mass m . In this figure the ϕ -axis and χ -axis correspond, however, this correspondence is dispensable. The strength of the Hawking radiation is independent of (θ, ϕ) and of ψ due to the spherical symmetry of the black hole and of the Hawking radiation. The disk-image is independent of χ because of the spherical symmetry. Each value of D ($< D_c$) is one-to-one corresponding to ω by the particle-geodesic when the particle-energy E ($> m$) is given.

3.1 Classification of Particle Trajectory

We rewrite the motion-equations (11) and (12) for the ballistic particle into the differential equations:

$$(\dot{y}^r)^2 = F^2 \left\{ 1 - \left(\frac{L}{E}\right)^2 \frac{F}{(y^r)^2} - \left(\frac{Y|\phi(y^r)|}{E}\right)^2 F \right\}, \quad (20)$$

$$\dot{y}^\varphi = \frac{L}{E} \frac{F}{(y^r)^2}. \quad (21)$$

We will abbreviate the particle-index i or flavor-index f in equations for simplicity. By combining the equations (20) and (21) a relation for the zenith-angle ω is obtained as

$$\tan \omega = r_{\text{BH}} \left. \frac{\partial y^\varphi}{\partial y^r} \right|_{y^r=r_{\text{BH}}} = \frac{L}{E} \frac{1}{r_{\text{BH}}}. \quad (22)$$

By using the relation (22) we employ the zenith-angle ω as a constant of the particle-motion instead of the angular momentum L . We approximate by

$$Y|\phi(r)| \simeq m \quad (23)$$

in the motion-equation (20) for simplifying the analysis, where m is the mass of the particle in the ordinary vacuum $\phi = v/\sqrt{2}$ [†]. By this approximation the backreaction from the Higgs-vev-structure into the particle-trajectories is ignored and the only influence of the radiated particles over the Higgs vev is considered. The equations of motion for the ballistic particle in (20) and (21) becomes

$$(\dot{y}^r)^2 = -W_{\text{eff}}(y), \quad (24)$$

$$\dot{y}^\varphi = \tan \omega \frac{r_{\text{BH}}}{(y^r)^2} F, \quad (25)$$

where we have defined an effective potential for the particle-motion

$$W_{\text{eff}}(y) := -F^2 \left\{ 1 - \tan^2 \omega \left(\frac{r_{\text{BH}}}{y^r}\right)^2 F - \left(\frac{m}{E}\right)^2 F \right\}. \quad (26)$$

The effective potential (26) is parameterized by two constants $(m/E, \omega)$.

According to the function-form of the effective potential (26), the parameter space $(m/E, \omega)$ is divided into the six regions; the Region-I, the Region-IIa, the Region-IIb, the Region-IIb+, the Region-IIb- and the Region-IIc. The division of the parameter space is shown in Figure 3. On each region the effective potential W_{eff} has different forms displayed in Figure 4. In the Region-I the particle radiated from the horizon runs away from the horizon to the infinite

[†]This approximation is available because the form of the final results $\phi(r)$ in Figure 9 are approximately flat.

distance because the effective potential W_{eff} never cross the zero level except for the horizon $r = r_{\text{BH}}$. In the Region-II's the radiated particle always turns its r -direction at each point satisfying $W_{\text{eff}}(r) = 0$ and returns into the horizon $r = r_{\text{BH}}$. The trajectory of the radiated particle is connected with the horizon and is described by each thick curve in Figure 4. In the Region-IIa and in the Region-IIc there is a trajectory disconnected from the horizon (the dotted curve in Figure 4). The trajectory disconnected from the horizon in the Region-IIc means the revolution-orbit around the black hole and that in the Region-IIa means the gravitational-scattering-trajectory by the black hole. Such trajectories disconnected from the horizon are not relevant to our subject.

In the Region-II's the relation among the turning point r_{turn} , the radiation angle ω and the ratio m/E is given by $W_{\text{eff}}(r_{\text{turn}}) = 0$ and it can be rewritten as

$$\tan^2 \omega = \tan^2 \omega_{\text{turn}} \left(r_{\text{turn}}, \frac{m}{E} \right), \quad (27)$$

where we have defined a function

$$\tan^2 \omega_{\text{turn}} \left(r_{\text{turn}}, \frac{m}{E} \right) := \left(\frac{r_{\text{turn}}}{r_{\text{BH}}} \right)^2 \left[\frac{1}{F(r_{\text{turn}})} - \left(\frac{m}{E} \right)^2 \right]. \quad (28)$$

We display the form of the function $\tan \omega_{\text{turn}}$ in Figure 5. When $0 \leq m/E < 1$, the relation (27) is valid for $r_{\text{BH}} < r_{\text{turn}} < r_{\text{c1}}(m/E)$ as the Region-IIa. When $1 \leq m/E < \sqrt{9/8}$, the relation (27) is valid for $r_{\text{BH}} < r_{\text{turn}} < r_{\text{c1}}(m/E)$ as the Region-IIc and the Region-IIb+ and for $r_{\text{cs}} < r_{\text{turn}} < r_{\text{c2}}(m/E)$ as the Region-IIb-. The relation (27) is not valid for $r_{\text{c1}} < r_{\text{turn}} < r_{\text{cs}}(m/E)$ because the relation indicates the turning radius of the revolution-orbit. We note that any particle with $1 \leq m/E < \sqrt{9/8}$ does not turn at the radius $r_{\text{c1}} < r < r_{\text{cs}}(m/E)$. When $\sqrt{9/8} \leq m/E$, the relation is valid for $r_{\text{BH}} < r_{\text{turn}} < r_{\text{c2}}(m/E)$ as the Region-IIb. We have defined the first maximum turning radius

$$r_{\text{c1}} \left(\frac{m}{E} \right) := \frac{r_{\text{BH}}}{1 - \left(\frac{m}{E} \right)^2} \left[\frac{3}{4} - \left(\frac{m}{E} \right)^2 + \frac{3}{4} \sqrt{1 - \frac{8}{9} \left(\frac{m}{E} \right)^2} \right] \quad (29)$$

for $0 < m/E < \sqrt{9/8}$ and its dual radius

$$r_{\text{c1Dual}} \left(\frac{m}{E} \right) := \frac{r_{\text{BH}}}{1 - \left(\frac{m}{E} \right)^2} \left[\frac{3}{4} - \left(\frac{m}{E} \right)^2 - \frac{3}{4} \sqrt{1 - \frac{8}{9} \left(\frac{m}{E} \right)^2} \right] \quad (30)$$

for $1 < m/E < \sqrt{9/8}$. These are given by the solutions of the quadratic equation

$$\left. \frac{\partial}{\partial r_{\text{turn}}} \tan^2 \omega_{\text{turn}} \right|_{r_{\text{turn}}=r_c} = 0. \quad (31)$$

We have also defined the second maximum turning radius

$$r_{c2}\left(\frac{m}{E}\right) := \frac{r_{\text{BH}}\left(\frac{m}{E}\right)^2}{\left(\frac{m}{E}\right)^2 - 1} \quad (32)$$

for $1 < m/E$ as a solution of $\tan^2 \omega(r_{c2}, m/E) = 0$ and have defined the splitting radius as

$$r_{\text{cs}} := \frac{r_{\text{BH}}}{\left(\frac{m}{E}\right)^2 - 1} \left[\frac{3}{2} - \left(\frac{m}{E}\right)^2 + \frac{3}{2} \sqrt{1 - \frac{8}{9} \left(\frac{m}{E}\right)^2} \right] \quad (33)$$

for $1 < m/E < \sqrt{9/8}$ as another solution of $\tan^2 \omega_{\text{turn}}(r_{\text{cs}}) = \tan^2 \omega_{\text{turn}}(r_{c1})$. The critical curve $\omega = \omega_c(m/E)$ which separates the Region-I from the Region-IIa in Figure 3 is given by

$$\begin{aligned} \tan^2 \omega_c\left(\frac{m}{E}\right) &:= \tan^2 \omega_{\text{turn}}\left(r_{c1}, \frac{m}{E}\right) \\ &= \frac{7}{2} - \left(\frac{m}{E}\right)^2 + \frac{1}{8} \frac{-1 + 27 \left[1 - \frac{8}{9} \left(\frac{m}{E}\right)^2\right]^{3/2}}{1 - \left(\frac{m}{E}\right)^2} \end{aligned} \quad (34)$$

where the right hand side is the function defined in (28). This critical curve also indicates the boundary which separates the Region-IIc from the Region-IIb-. This critical curve is defined for $0 \leq m/E \leq \sqrt{9/8}$. The other boundary which separates the Region-IIc from the Region-IIb+ is given by

$$\begin{aligned} \tan^2 \omega_{\text{cDual}}\left(\frac{m}{E}\right) &:= \tan^2 \omega\left(r_{\text{c1Dual}}, \frac{m}{E}\right) \\ &= \frac{7}{2} - \left(\frac{m}{E}\right)^2 + \frac{1}{8} \frac{-1 - 27 \left[1 - \frac{8}{9} \left(\frac{m}{E}\right)^2\right]^{3/2}}{1 - \left(\frac{m}{E}\right)^2} \end{aligned} \quad (35)$$

which is defined for $1 < m/E \leq \sqrt{9/8}$.

3.2 Density Distribution as Functional of Flux

We consider the density-distribution $\mathcal{N}_f(E, r)$. The density-distribution is a functional of the flux $f(E, \omega)$ on the horizon and is also a function of both the parameter m_f/E and the position r , then we rewrite the density-distribution as $\mathcal{N}(m/E, r; f)$ in this subsection. The particle-density at the position r is the superposition of the density of the particles which can reach the position r . When we put values of both the radiation angle ω and the parameter m/E , we find whether the particle can reach the position r or not. A contribution to the density by a particle is inversely proportional to its velocity \dot{y}^r . Therefore the particle-number-density is calculated by integrating out the product of the flux $f(E, \omega)$ on the horizon, the geometrical

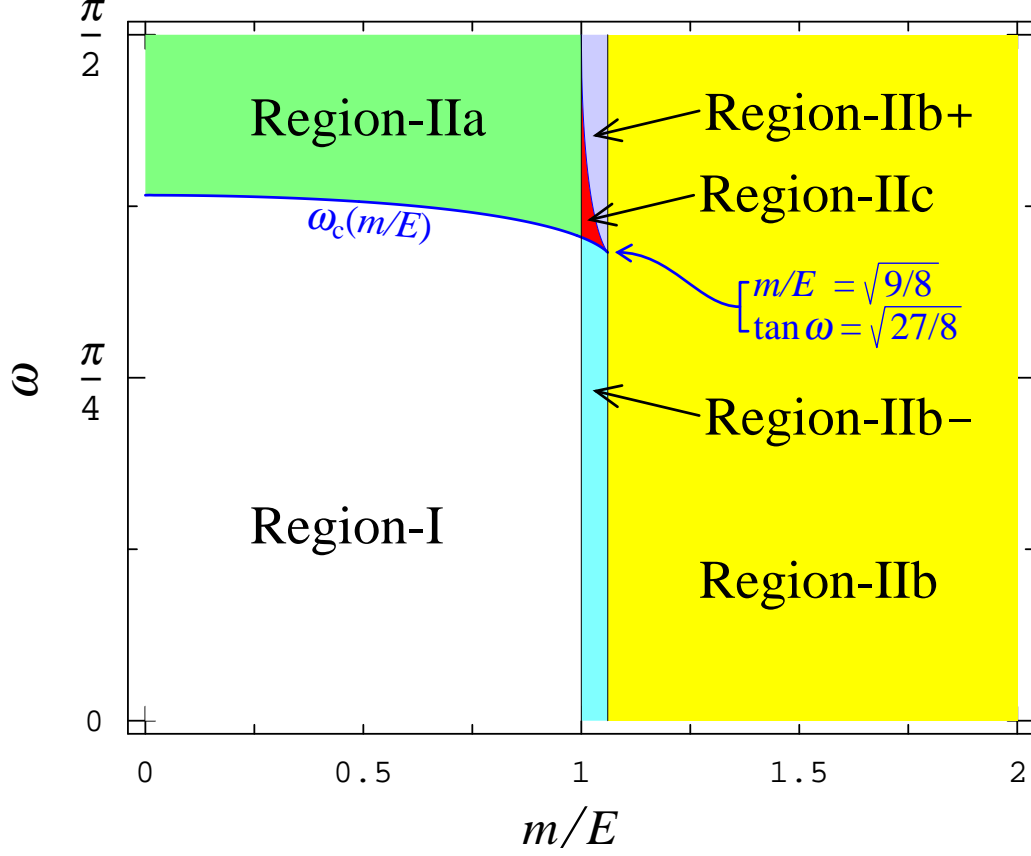


Figure 3: Parameter space $(m/E, \omega)$ of the effective potential W_{eff} for the ballistic particle. The space is classified into six regions; Region-I, Region-IIa, Region-IIb, Region-IIb+, Region-IIb- and Region-IIc. The typical forms of the effective potential corresponding to the regions are shown in Figure 4. The radiated particle runs away from the horizon in the Region-I. In the other regions (Region-II's), any radiated particle returns into the horizon. The Region-I is bounded on both the curve $\omega_c(m/E)$ in (34) by the Region-IIa and the line $m/E = 1$ by the Region-IIb-. We note $\tan \omega_c(0) = \sqrt{27/4}$ and $\tan \omega_c(1) = 2$. The Region-IIc is bounded on the curve $\omega_{c\text{Dual}}(m/E)$ in (35) by the Region-IIb+, on the curve $\omega_c(m/E)$ by the Region-IIb- and on the line $m/E = 1$ by the Region-IIa. The Region-IIb is bounded on the line $m/E = \sqrt{9/8}$.

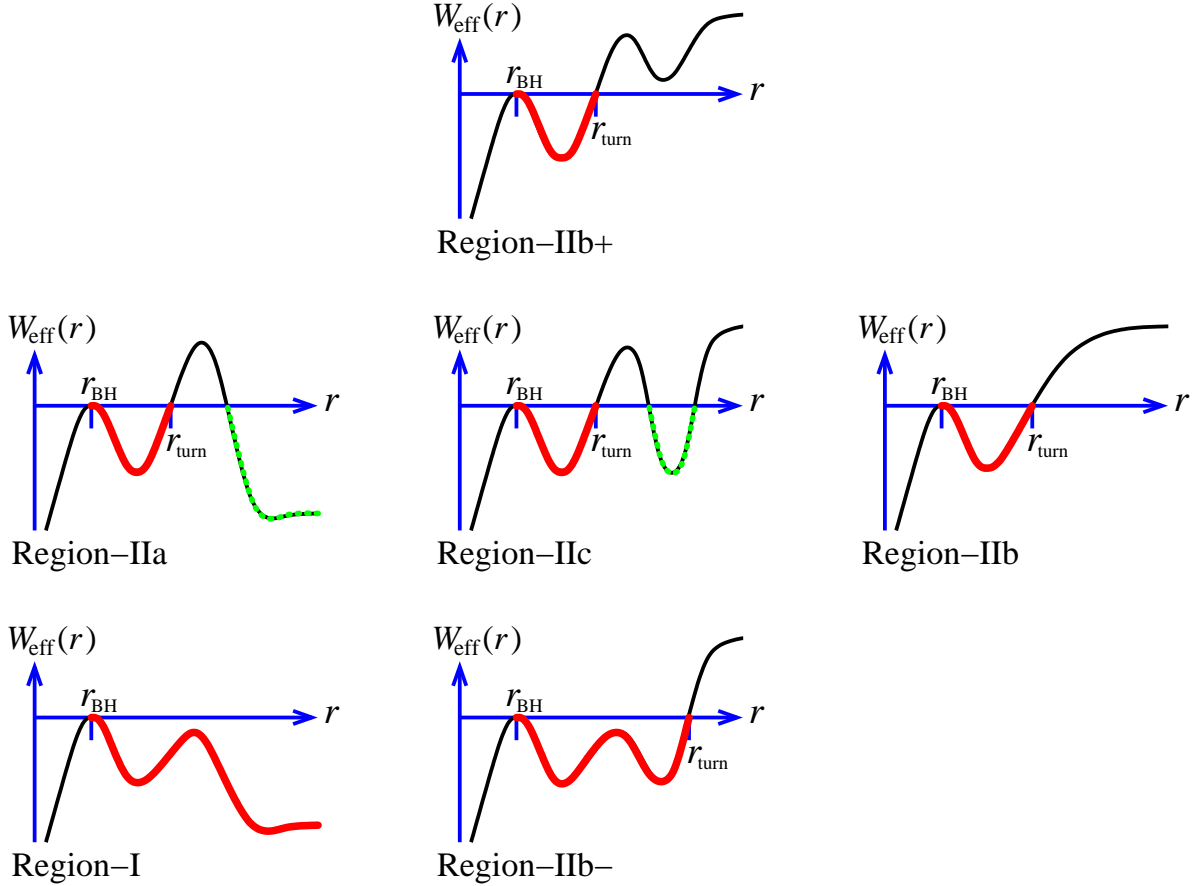


Figure 4: Typical forms of the effective potential $W_{\text{eff}}(r)$ in (26) for the six parameter regions. The figures are arranged for corresponding to the position of each region in the parameter space in Figure 3. The curve is the function-form of the effective potential $W_{\text{eff}}(r)$ for the ballistic particle and the motion of the particle is allowed for $W_{\text{eff}}(r) \leq 0$. The thick curve means the trajectory of particle-motion which is connected to the horizon. The motion of Hawking-radiated particle is described by the thick curves. The dotted curves mean the particle-trajectories disconnected to the horizon, i.e., the gravitational bending in the Region-IIa and the revolution-orbit in the Region-IIc, and is not relevant to our subject. In the Region-I the radiated particle runs away from the horizon into the infinite distance. In the Region-II's the radiated particle turns its r -direction at the radius $r = r_{\text{turn}}$ and returns into the horizon $r = r_{\text{BH}}$.

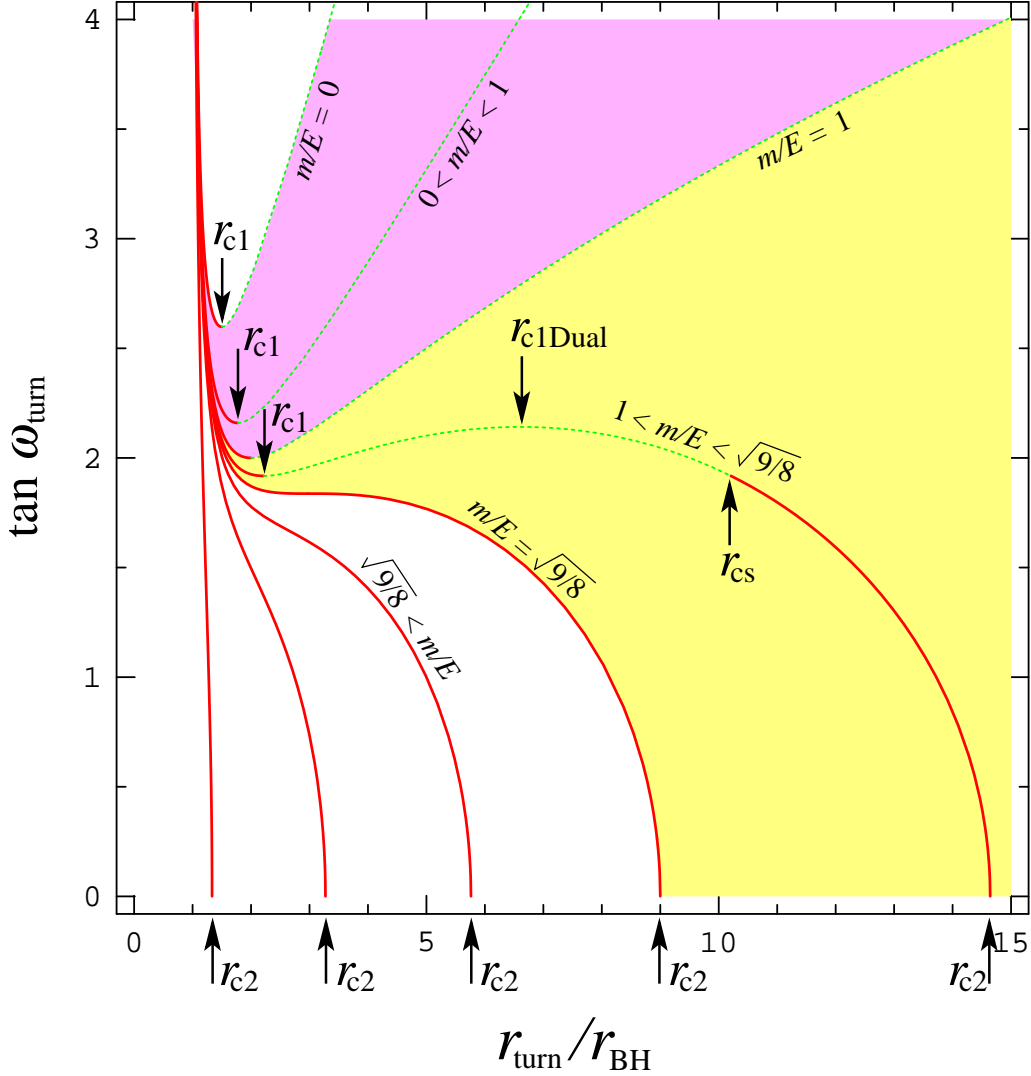


Figure 5: The function-forms of $\tan \omega_{\text{turn}}(r_{\text{turn}}, m/E)$ defined in (28) for various values of $m/E > 0$. The forms of the curve are classified into three classes $0 \leq m/E \leq 1$, $1 < m/E < \sqrt{9/8}$ and $\sqrt{9/8} \leq m/E$. The curve gives us the relation between the turning radius r_{turn} and the radiation-zenith-angle $\tan \omega = \tan \omega_{\text{turn}}(r_{\text{turn}}, m/E)$. For given ω , the solution r nearest the horizon becomes the true turning radius r_{turn} . Then solid curve is the turning radius r_{turn} and the dotted curve means a fake. For $0 \leq m/E < \sqrt{9/8}$, the solid curve is bounded on $r_{\text{turn}} = r_{c1}$ which is the first maximum turning radius whose value is given in (29). On $\omega_{\text{turn}} = 0$, the solid curve is also bounded on $r_{\text{turn}} = r_{c2}$ which is the second maximum turning radius (32). For $1 < m/E < \sqrt{9/8}$, we have another bound on $r_{\text{turn}} = r_{cs}$ which is the splitting radius (33).

factor $(r_{\text{BH}}/r)^2$ and the inverse velocity $1/\dot{y}^r$ with the integral variable ω . Here we define the function

$$\mathcal{N}_{\omega_1}^{\omega_2}(m/E, r; f) := \left(\frac{r_{\text{BH}}}{r}\right)^2 \int_{\omega_1}^{\omega_2} d\omega \sin \omega \int_0^{2\pi} d\psi \frac{f(E, \omega)}{\dot{y}^r(r, \omega, m/E)} \quad (36)$$

for convenience. Because a part of the parameter space $(m/E, \omega)$ contributes to the density-distribution $\mathcal{N}(m/E, r; f)$ at the position r , the integral interval $[\omega_1, \omega_2]$ for the density-distribution $\mathcal{N}(m/E, r; f)$ should be carefully chosen, i.e., the integral interval $[\omega_1, \omega_2]$ depends on the position r and on the parameter m/E . The density-distribution is given by the sum of contributions from the parameter regions:

$$\mathcal{N}\left(\frac{m}{E}, r; f\right) = \mathcal{N}_{\text{I}}\left(\frac{m}{E}, r; f\right) + \mathcal{N}_{\text{IIa}}\left(\frac{m}{E}, r; f\right) + \mathcal{N}_{\text{IIb}}\left(\frac{m}{E}, r; f\right) + \mathcal{N}_{\text{IIb}\pm, c}\left(\frac{m}{E}, r; f\right) \quad (37)$$

$\mathcal{N}_{\text{I}}(m/E, r; f)$ is the density-distribution contributed by the Region-I, $\mathcal{N}_{\text{IIa}}(m/E, r; f)$ is that by the Region-IIa, $\mathcal{N}_{\text{IIb}}(m/E, r; f)$ is that by the Region-IIb and $\mathcal{N}_{\text{IIb}\pm, c}(m/E, r; f)$ is that by the combination of the Region-IIb-, the Region-IIb+ and the Region-IIc. These density-distributions are given by the function (36) with a suitable integral interval $[\omega_1, \omega_2]$. The density-distributions $\mathcal{N}_{\text{I}}(m/E, r; f)$, $\mathcal{N}_{\text{IIa}}(m/E, r; f)$, $\mathcal{N}_{\text{IIb}}(m/E, r; f)$ and $\mathcal{N}_{\text{IIb}\pm, c}(m/E, r; f)$ are considered as follows respectively.

1) The density-distribution contributed by the Region-I.

This parameter-region is given by $0 \leq m/E < 1$ and $0 \leq \omega < \omega_c(m/E)$ (see Figure 3). The radiated particle in this region runs away from the horizon $r = r_{\text{BH}}$ to the infinite distance $r = \infty$ and never turns its r -direction (see Figure 4). Therefore the integral interval is given by $0 \leq \omega < \omega_c(m/E)$ and this interval does not depend on the position r . The density-distribution becomes

$$\mathcal{N}_{\text{I}}\left(\frac{m}{E}, r; f\right) = \begin{cases} \mathcal{N}_0^{\omega_c(\frac{m}{E})}\left(\frac{m}{E}, r; f\right) & \left(0 \leq \frac{m}{E} < 1 \text{ and } r_{\text{BH}} < r \leq \infty\right) \\ 0 & \text{(others)} \end{cases} \quad (38)$$

2) The density-distribution contributed by the Region-IIa.

This region is given by $0 \leq m/E < 1$ and $\omega_c(m/E) \leq \omega < \pi/2$ (see Figure 3). The radiated particle runs away from the horizon $r = r_{\text{BH}}$, turns its r -direction at radius $r = r_{\text{turn}}$ which depends on the zenith-angle ω and returns into the horizon. (see Figure 4). Then the integral interval $[\omega_1, \omega_2]$ depends on the position r . The particle within the parameter region $\omega_c(m/E) \leq \omega \leq \omega_{\text{turn}}(r, m/E)$ can reach the position r and contributes to the density-distribution $\mathcal{N}_{\text{IIa}}(m/E, r; f)$ because a particle with the zenith-angle $\omega = \omega_{\text{turn}}(r, m/E)$ turns its r -direction at the position r . On the other hand, the particle within the parameter region $\omega_{\text{turn}}(r, m/E) < \omega < \pi/2$ cannot reach the position r and does not contribute to the density-distribution $\mathcal{N}_{\text{IIa}}(m/E, r; f)$. Therefore the integral interval should be $\omega_c(m/E) \leq \omega \leq$

$\omega_{\text{turn}}(r, m/E)$ which is depending on the position r and the density-distribution becomes

$$\mathcal{N}_{\text{IIa}}\left(\frac{m}{E}, r; f\right) = \begin{cases} 2 \times \mathcal{N}_{\omega_c(\frac{m}{E})}^{\omega_{\text{turn}}(r, \frac{m}{E})}\left(\frac{m}{E}, r; f\right) & \left(0 \leq \frac{m}{E} < 1 \text{ and } r_{\text{BH}} < r \leq r_{\text{c1}}\left(\frac{m}{E}\right)\right) \\ 0 & \text{(others)} \end{cases} \quad (39)$$

We need the factor two in this form because both the go and the return of the particle contribute to the density-distribution. Any particle in the Region-IIa does not contribute to the density-distribution for $r > r_{\text{c1}}\left(\frac{m}{E}\right)$ because the maximum turning radius in the Region-IIa is given by $r_{\text{c1}}\left(\frac{m}{E}\right)$ and particle does not turn on the radius $r > r_{\text{c1}}\left(\frac{m}{E}\right)$. Then the integral form in (39) is restricted to $r_{\text{BH}} < r < r_{\text{c1}}\left(\frac{m}{E}\right)$. For example we obtain $\tan \omega_c = \sqrt{\frac{27}{4}}$ and $r_{\text{c1}} = (3/2)r_{\text{BH}}$ when we consider massless particle $m = 0$. We obtain $\tan \omega_c = 2$ and $r_{\text{c1}} = 2r_{\text{BH}}$ for the particle with $m/E = 1$.

3) The density-distribution contributed by the Region-IIb.

This region is given by $\sqrt{9/8} \leq m/E$ and $0 \leq \omega < \pi/2$. The particle whose zenith-angle satisfies $0 \leq \omega \leq \omega_{\text{turn}}\left(r, \frac{m}{E}\right)$ can reach the position r because the radiated particle with the zenith-angle $\omega = \omega_{\text{turn}}\left(r, \frac{m}{E}\right)$ turns its r -direction at the position r . The density at r is given by the integration over the radiation angle $0 \leq \omega \leq \omega_{\text{turn}}\left(r, \frac{m}{E}\right)$. We obtain

$$\mathcal{N}_{\text{IIb}}\left(\frac{m}{E}, r; f\right) = \begin{cases} 2 \times \mathcal{N}_0^{\omega_{\text{turn}}(r, \frac{m}{E})}\left(\frac{m}{E}, r; f\right) & \left(\sqrt{\frac{9}{8}} \leq \frac{m}{E} \text{ and } r_{\text{BH}} < r \leq r_{\text{c2}}\left(\frac{m}{E}\right)\right) \\ 0 & \text{(others)} \end{cases} \quad (40)$$

The integral form in (40) is restricted to $r_{\text{BH}} < r \leq r_{\text{c2}}\left(\frac{m}{E}\right)$ because the maximum turning radius in this region is given by $r_{\text{c2}}\left(\frac{m}{E}\right)$ rather than $r_{\text{c1}}\left(\frac{m}{E}\right)$ (see the curves with $\sqrt{9/8} \leq m/E$ in Figure 5). For example, we have $r_{\text{c2}} = 9r_{\text{BH}}$ for the particle with $m/E = \sqrt{9/8}$ and we have $r_{\text{c2}} \rightarrow 1$ for the particle with the limit $m/E \rightarrow \infty$.

4) The density-distribution contributed by the Region-IIb \pm and the Region-IIc.

The parameter-region is simply given by $1 \leq m/E < \sqrt{9/8}$ and $0 \leq \omega < \pi/2$, however, the analysis becomes a little complicated and more careful treatment is required because the region is composed of three Regions (IIb+, IIb- and IIc) due to the revolution-orbit in the Region-IIc, which is irrelevant to our subject. Each particle radiated from the horizon with zenith-angle ω turns its r -direction at the position r_{turn} and returns into the horizon. The relation between ω and r_{turn} is given by the equation (27) (also see Figure 5). In the region-IIb- ($\omega \leq \omega_c(\frac{m}{E}) := \omega_{\text{turn}}(r_{\text{c1}}, \frac{m}{E})$) and in the region-IIb+ ($\omega > \omega_{\text{cDual}}(\frac{m}{E}) := \omega_{\text{turn}}(r_{\text{c1Dual}}, \frac{m}{E})$), we have a unique solution r_{turn} of the equation (27) for the fixed ω . On the other hand, in the region-IIc ($\omega_c < \omega \leq \omega_{\text{turn}}(r_{\text{c1Dual}})$) there are three solutions of the equation (27) (see Figure 4 and Figure 5) because the revolution-orbit around the black hole is also allowed. The solution nearest to the horizon should be selected as r_{turn} because the revolution-orbit which

is disconnected with the horizon is not relevant to the Hawking radiation and the trajectory of the Hawking radiation is connected to the horizon.

When the zenith-angle ω becomes larger from zero to $\omega_c(m/E)$ in the considering region $1 \leq m/E < \sqrt{9/8}$, the turning radius r_{turn} becomes smaller. When ω equals to $\omega_c(m/E)$, the turning radius r_{turn} discontinuously jumps from the radius r_{cs} to the smaller radius r_{c1} (see the curve with $1 < m/E < \sqrt{9/8}$ in Figure 5) because the parameter region is changed from the Region-IIb- into Region-IIc. At the moment the trajectory is separated into the two disconnected parts and one of the trajectories becomes the revolution-orbit which is irrelevant (see the difference between $W_{\text{eff}}(r)$ in the Region-IIb- and that in Region-IIc in Figure 4). When ω becomes large from $\omega_c(m/E)$ to $\pi/2$, the turning radius r_{turn} becomes small continuously and approaches the horizon radius r_{BH} . Noting special happens in the transition from the Region-IIc into the Region-IIb+ except for the disappearance of the revolution-orbit which is not relevant.

To consider the density-distribution at the position r , we should consider which particle can reach the position r . When $r_{\text{cs}}(\frac{m}{E}) \leq r \leq r_{\text{c2}}(\frac{m}{E})$, the particle belongs to the Region-IIb-. The particle radiated with the zenith-angle $\omega = \omega_{\text{turn}}(r, \frac{m}{E})$ turns its r -direction at the position r , then the particle with $0 \leq \omega \leq \omega_{\text{turn}}(r, \frac{m}{E})$ can reach the position r . The density at r is given by the integration over the radiation angle $0 \leq \omega \leq \omega_{\text{turn}}(r, \frac{m}{E})$. When $r_{\text{c1}}(\frac{m}{E}) < r < r_{\text{cs}}(\frac{m}{E})$, the particle still belongs to the Region-IIb-. The radiated particle does not turn in the region $r_{\text{c1}}(\frac{m}{E}) < r < r_{\text{cs}}(\frac{m}{E})$ and always turns at $r = r_{\text{cs}}(\frac{m}{E})$. Then the integral-interval should be $0 \leq \omega \leq \omega_{\text{turn}}(r_{\text{cs}}, \frac{m}{E})$. The integral-interval can be rewritten as $0 \leq \omega \leq \omega_c(\frac{m}{E})$ by using the definition of $\omega_c(\frac{m}{E})$ in (34). When $r_{\text{BH}} < r \leq r_{\text{c1}}(\frac{m}{E})$, the particle which belongs to the Region-IIc or the Region-IIb+ begins to contribute the density-distribution. The situation is essentially same to the Region-IIb- for $r_{\text{cs}}(\frac{m}{E}) \leq r \leq r_{\text{c2}}(\frac{m}{E})$ and the integral interval is also given by $0 \leq \omega \leq \omega_{\text{turn}}(r, \frac{m}{E})$. The density-distribution for $1 \leq m/E < \sqrt{9/8}$ is summarized as

$$\mathcal{N}_{\text{IIb}\pm, \text{c}}\left(\frac{m}{E}, r; f\right) = \begin{cases} 0 & \left(r_{\text{c2}}\left(\frac{m}{E}\right) < r \leq \infty\right) \\ 2 \times \mathcal{N}_0^{\omega_{\text{turn}}\left(r, \frac{m}{E}\right)}\left(\frac{m}{E}, r; f\right) & \left(r_{\text{cs}}\left(\frac{m}{E}\right) \leq r \leq r_{\text{c2}}\left(\frac{m}{E}\right)\right) \\ 2 \times \mathcal{N}_0^{\omega_c\left(\frac{m}{E}\right)}\left(\frac{m}{E}, r; f\right) & \left(r_{\text{c1}}\left(\frac{m}{E}\right) < r < r_{\text{cs}}\left(\frac{m}{E}\right)\right) \\ 2 \times \mathcal{N}_0^{\omega_{\text{turn}}\left(r, \frac{m}{E}\right)}\left(\frac{m}{E}, r; f\right) & \left(r_{\text{BH}} < r \leq r_{\text{c1}}\left(\frac{m}{E}\right)\right) \end{cases}. \quad (41)$$

The resultant form (41) has a little complicated conditions for r , however, the form is a continuous function of r because the integral interval continuously changes as r changes.

4 Radiation Angle Distribution

In this section we consider the particle-flux on the horizon $f(E, \omega)$ in (19), which is required to evaluate the particle density-distribution $\mathcal{N}(m/E, r; f)$ in (37).

As a consequence of the assumption-(i) which is mentioned in the previous section and of the spherical symmetry, the observer at the infinite distance finds a disk image as a detection of the Hawking-radiated particles. In Figure 2 the correspondence of a particle-geodesic to a point in the image of the radiation on the screen at the infinite distance is schematically shown. The observed image is equal to the image on the screen. The screen is parameterized by the polar coordinate (D, χ) , where the parameter D is distance from the center of the screen. The parameter D can be regard the impact parameter of an absorption-process into the black hole because the absorption of the particle is regarded as the inverse process of the Hawking radiation. A relation

$$\frac{L}{E} = v_\infty D, \quad (42)$$

is derived from conservation of the angular momentum of the particle, where velocity of the particle at the infinite distance

$$v_\infty \left(\frac{m}{E} \right) := \sqrt{1 - \left(\frac{m}{E} \right)^2} \quad (43)$$

is defined. The particle which reaches the infinite distance satisfies a condition $E > m$. By combining (43) with (22) we obtain the relation between the radiation-zenith-angle ω and the impact parameter D as

$$D \left(\frac{m}{E}, \omega \right) = r_{\text{BH}} \frac{\tan \omega}{v_\infty}. \quad (44)$$

In order for a radiated particle to reach the infinite distance, the radiation-zenith-angle should satisfy $0 \leq \tan \omega < \tan \omega_c \left(\frac{m}{E} \right)$. This restriction for the radiation-zenith-angle ω is corresponding to the restriction for the impact parameter $0 \leq D < D_c \left(\frac{m}{E} \right)$. By using the relation between ω and D in (44), we obtain the radius of the apparent disk-image on the screen as

$$D_c \left(\frac{m}{E} \right) := r_{\text{BH}} \frac{\tan \omega_c}{v_\infty}. \quad (45)$$

Therefore the impact parameter D , namely the position of the image, is one-to-one corresponding to the radiation-zenith-angle ω if $D < D_c(m/E)$ and $E > m$ are satisfied.

The apparent disk area

$$\sigma_{\text{BH}} \left(\frac{m}{E} \right) := \pi D_c^2 \left(\frac{m}{E} \right) \quad (46)$$

means the absorption-cross-section of the black hole for the particle in the ballistic picture (eikonal limit). The area of the disk is depending on m/E . For example we have $D_c = \sqrt{\frac{27}{4}} r_{\text{BH}}$ and $\sigma_{\text{BH}} = \frac{27}{4} \pi r_{\text{BH}}^2$ for massless particles.

Because the Hawking radiation for the observer at the infinite distance is regarded as an inverse process of the particle-absorption into the horizon, the differential luminosity of the Hawking radiation is given by the product of the absorption-cross-section and the thermal flux from the black body per unit area:

$$dL(T_{\text{BH}}, m, E) = \begin{cases} \sigma_{\text{BH}}\left(\frac{m}{E}\right) \times \frac{v_{\infty}}{4} \times \frac{g}{(2\pi)^3} f_{T_{\text{BH}}}(E) 4\pi E^2 v_{\infty} dE & (E > m) \\ 0 & (E < m) \end{cases}, \quad (47)$$

where

$$f_{T_{\text{BH}}}(E) := \frac{1}{e^{\frac{E}{T_{\text{BH}}}} \pm 1} \quad (48)$$

is the Fermi-Dirac or the Bose-Einstein distribution-function for the Hawking temperature T_{BH} and g is the degree of the freedom for the particle on the temperature T_{BH} . The absorption-cross-section $\sigma_{\text{BH}}\left(\frac{m}{E}\right)$ in the luminosity dL is depending on the particle-energy E . This dependency is referred as “the gray body factor” of the Hawking radiation [1, 2, 10]. We have a relation between the flux on the horizon $f(E, \omega)$ in (19) and the differential luminosity (47):

$$4\pi r_{\text{BH}}^2 \int d\mathcal{F} = 4\pi r_{\text{BH}}^2 \int_0^{\omega_c} d\omega \sin \omega \int_0^{2\pi} d\chi f(E, \omega) dE = dL(T_{\text{BH}}, m, E). \quad (49)$$

This relation gives us a restriction for the flux $f(E, \omega)$.

To determine the flux $f(E, \omega)$, we assume

- (ii) the brightness of the disk-image for each particle-energy appears to be uniform over the disk-image for the observer at the infinite distance and the energy-spectrum of the disk-image is given by the perfect black body radiation with the Hawking temperature.

By the above assumption and the relation (44) we have the relation between the differential brightness of the disk (47) and the flux on the horizon as

$$\begin{aligned} & \frac{v_{\infty}}{4} \times \frac{g_f}{(2\pi)^3} f_{T_{\text{BH}}}(E) 4\pi E^2 v_{\infty} dE \times (dD D d\chi) \\ = & 4\pi r_{\text{BH}}^2 \times \left[\frac{1}{4\pi \cos^3 \omega} \times \frac{1}{4} \frac{g_f}{(2\pi)^3} f_{T_{\text{BH}}}(E) 4\pi E^2 dE \right] \times (d\omega \sin \omega d\chi). \end{aligned} \quad (50)$$

By using the spherical symmetry of the Hawking radiation, $(d\omega \sin \omega d\chi)$ in the right hand side of (50) can be rewritten to $(d\omega \sin \omega d\psi)^{\ddagger}$. By comparing with the definition of the particle-flux in (19), we obtain the particle-flux on the horizon per unit area

$$f(E, \omega) = \frac{1}{16\pi \cos^3 \omega} \times \frac{g}{(2\pi)^3} f_{T_{\text{BH}}}(E) 4\pi E^2. \quad (51)$$

[‡] $d\chi$ is equal to $d\phi$ due to the configuration in Figure 2. $d\phi$ can be regard as $d\psi$ because both the space-time and the Hawking-radiation are spherical symmetric then ϕ -axis is exchangeable for ψ -axis.

The resultant flux (51) satisfies the restriction in (49).

We should note that the resultant flux (51) is defined for the particles which belong to the Region-I because the particles in Region-II's cannot reach the observer. Namely, the flux (51) is only defined for high elevation-angle[§] $0 \leq \omega < \omega_c$ and high particle-energy $E > m_f$. We need the flux $f(E, \omega)$ defined for all elevation-angle $0 \leq \omega < \pi/2$ and for all particle-energy $0 \leq E \leq \infty$ to calculate the particle number density $\mathcal{N}(m/E, r; f)$. To solve the problem we perform a analytic continuation of the flux, namely, we extend the domain of the flux (51) to all elevation-angle $0 \leq \omega < \pi/2$ and all particle-energy $0 \leq E \leq \infty$ with keeping the function form of the flux (51). The analytic continuation can be performed C^∞ -smoothly because no singularity exists in the new domain of definition. The resultant flux (51) defined for $0 \leq \omega < \pi/2$ diverges on $\omega = \pi/2$.

The radiation-flux on the normal black body with temperature T_{BH} is given by

$$f(E, \omega) = \frac{\cos \omega}{4\pi} v^2 \times \frac{g}{(2\pi)^3} f_{T_{\text{BH}}}(E) 4\pi E^2. \quad (52)$$

Our resultant flux on the horizon (51) is different from the flux (52). Especially the dependence on the radiation-zenith-angle ω is quite different. We find the low-elevation-angle-dominance of the flux on the horizon. The dependence on the particle-velocity is also different.

5 Density of the Ballistic Particles II

We concretely calculate the particle-density-distribution (37) by using the resultant flux on the horizon (51). We prepare several functions to calculate the density-distribution (37). By substituting the flux $f(E, \omega)$ resulted in (51) into the functional $\mathcal{N}_{\omega_1}^{\omega_2}(m/E, r; f)$ in (36), we obtain

$$\begin{aligned} \mathcal{N}_{\omega_1}^{\omega_2}(m/E, r) &= \frac{1}{16\pi} \frac{g}{(2\pi)^3} f_{T_{\text{BH}}}(E) 4\pi E^2 \left(\frac{r_{\text{BH}}}{r}\right)^2 \int_{\omega_1}^{\omega_2} d\omega \int_0^{2\pi} d\chi \frac{\sin \omega}{\cos^3 \omega} \frac{1}{\dot{y}^r(r, \omega, m/E)} \\ &= \frac{1}{8} \frac{g}{(2\pi)^3} f_{T_{\text{BH}}}(E) 4\pi E^2 \left(\frac{r_{\text{BH}}}{r}\right)^2 \frac{1}{F(r)} \tilde{G}_{\omega_1}^{\omega_2}(A, B), \end{aligned} \quad (53)$$

where we have defined

$$\tilde{G}_{\omega_1}^{\omega_2}(A, B) := \int_{\omega_1}^{\omega_2} d\omega \frac{\sin \omega}{\cos^3 \omega} \frac{1}{\sqrt{B - A \tan^2 \omega}} \quad (54)$$

$$A := \left(\frac{r_{\text{BH}}}{r}\right)^2 F(r) \quad (55)$$

$$B := 1 - \left(\frac{m}{E}\right)^2 F(r). \quad (56)$$

[§]The elevation-angle of the radiation is defined as $(\pi/2 - \omega)$. High elevation-angle means small zenith-angle $\omega \sim 0$ and low elevation-angle means large zenith-angle $\omega \sim \pi/2$.

The definite integration in (54) can be performed as

$$\tilde{G}_{\omega_1}^{\omega_2}(A, B) := \tilde{G}_{\omega_1}(A, B) - \tilde{G}_{\omega_2}(A, B), \quad (57)$$

where

$$\tilde{G}_\omega := \frac{1}{A} \sqrt{B - A \tan^2 \omega} \quad (58)$$

is a primitive function of the integrand. For convenience of the following calculations we show several evaluations of the primitive function (58):

$$\tilde{G}_0 = \frac{1}{F} \left(\frac{r}{r_{\text{BH}}} \right)^2 \sqrt{1 - \left(\frac{m}{E} \right)^2 F(r)} \quad (59)$$

$$\tilde{G}_{\omega_c(\frac{m}{E})} = \frac{1}{F} \left(\frac{r}{r_{\text{BH}}} \right)^2 \frac{|r - r_{\text{c1}}|}{r} \sqrt{\left\{ \left(\frac{m}{E} \right)^2 - 1 \right\} \frac{r_{\text{cs}} - r}{r}} \quad (60)$$

$$\tilde{G}_{\omega_{\text{turn}}(r, \frac{m}{E})} = 0. \quad (61)$$

We rewrite the density-distribution $\mathcal{N}(E, r; f)$ in (37) as

$$\mathcal{N}(E, r) = \frac{1}{4} \frac{g}{(2\pi)^3} f_{T_{\text{BH}}}(E) 4\pi E^2 \times \left(\frac{r_{\text{BH}}}{r} \right)^2 \frac{1}{F^2(r)} \frac{1}{2} G \left(\frac{m}{E}, r \right), \quad (62)$$

where we have defined a dimensionless positive function G as

$$G \left(\frac{m}{E}, r \right) = G_{\text{I}} \left(\frac{m}{E}, r \right) + G_{\text{IIa}} \left(\frac{m}{E}, r \right) + G_{\text{IIb}\pm, c} \left(\frac{m}{E}, r \right) + G_{\text{IIb}} \left(\frac{m}{E}, r \right). \quad (63)$$

The functions $G_{\text{I}}, G_{\text{IIa}}, G_{\text{IIb}\pm, c}$ and G_{IIb} are corresponding to the partial density-distributions $\mathcal{N}_{\text{I}}, \mathcal{N}_{\text{IIa}}, \mathcal{N}_{\text{IIb}\pm, c}$ and \mathcal{N}_{IIb} in (37). The relation between G 's and \mathcal{N} 's is also given by (62). The factors before a symbol of the first product in (62) correspond to the number-density of the particles radiated from the normal black body with temperature T_{BH} . The factor $(r_{\text{BH}}/r)^2$ is a geometrical factor of spherical source of the radiation. The factor $1/F^2(r)$ means a principal general relativistic effect and plays important role near the horizon. The factor $G/2$ means a residual correction including the finite mass effects. We can show that $G/2$ is regular function and have finite value $G(r_{\text{BH}})/2 = 1$ on the horizon. We can also show that G is finite for all position r except for $G(1, r \rightarrow \infty)$. Therefore the density-distribution (62) is governed by the factor $1/F^2(r)$ near the horizon. When $m < E$, the density-distribution (62) is governed by the factor $(r_{\text{BH}}/r)^2$ for distant region.

We concretely calculate the correction factors $G_{\text{I}}, G_{\text{IIa}}, G_{\text{IIb}\pm, c}$ and G_{IIb} by using the relations (59), (60) and (61). From (38) we obtain

$$G_{\text{I}} \left(\frac{m}{E}, r \right) = \left(\frac{r}{r_{\text{BH}}} \right)^2 \left[\sqrt{1 - \left(\frac{m}{E} \right)^2 F} - \frac{|r - r_{\text{c1}}|}{r} \sqrt{\left\{ \left(\frac{m}{E} \right)^2 - 1 \right\} \frac{r_{\text{cs}} - r}{r}} \right] \quad (64)$$

for $r_{\text{BH}} \leq r \leq \infty$. We find

$$\lim_{r \rightarrow \infty} G_{\text{I}} \left(\frac{m}{E}, r \right) = \frac{\tan \omega_c^2 \left(\frac{m}{E} \right)}{v_\infty} \quad (65)$$

and it is consistent with the relation

$$\lim_{r \rightarrow \infty} \frac{dL}{4\pi r^2} = \lim_{r \rightarrow \infty} v_\infty \mathcal{N} dE \quad (66)$$

between (47) and (62). From (39) we obtain

$$G_{\text{IIa}} \left(\frac{m}{E}, r \right) = \begin{cases} 2 \times \left(\frac{r}{r_{\text{BH}}} \right)^2 \frac{|r-r_{\text{c1}}|}{r} \sqrt{\left\{ \left(\frac{m}{E} \right)^2 - 1 \right\} \frac{r_{\text{cs}}-r}{r}} & (r_{\text{BH}} \leq r \leq r_{\text{c1}}) \\ 0 & (r_{\text{c1}} < r \leq \infty) \end{cases} \quad (67)$$

By using the property of the absolute-value function in (64) and (67), we can summarize

$$G_{\text{I+IIa}} \left(\frac{m}{E}, r \right) := G_{\text{I}} \left(\frac{m}{E}, r \right) + G_{\text{IIa}} \left(\frac{m}{E}, r \right) \quad (68)$$

$$= \left(\frac{r}{r_{\text{BH}}} \right)^2 \left[\sqrt{1 - \left(\frac{m}{E} \right)^2} F - \frac{r - r_{\text{c1}}}{r} \sqrt{\left\{ \left(\frac{m}{E} \right)^2 - 1 \right\} \frac{r_{\text{cs}} - r}{r}} \right]. \quad (69)$$

as the G -function for $0 \leq m/E < 1$ and $r_{\text{BH}} \leq r \leq \infty$. Both G_{I} and G_{IIa} as a function of r are non-differentiable at $r = r_{\text{c1}}$, however, the function $G_{\text{I+IIa}}$ becomes differentiable at $r = r_{\text{c1}}$. The function $G_{\text{I+IIa}}$ is smooth and monotonously increasing function for $r_{\text{BH}} \leq r \leq \infty$. The function has the lower bound 2 for $r = r_{\text{BH}}$ and the upper bound (65). The function $G_{\text{I+IIa}}$ is almost flat for $r \gg r_{\text{BH}}$ except for $m/E = 1$, then it can be approximated with $G_{\text{I+IIa}}(m/E, r) \simeq G_{\text{I}}(m/E, \infty)$ for $r \gg r_{\text{BH}}$.

From (40) we obtain

$$G_{\text{IIb}} \left(\frac{m}{E}, r \right) = \begin{cases} 2 \times \left(\frac{r}{r_{\text{BH}}} \right)^2 \sqrt{1 - \left(\frac{m}{E} \right)^2} F(r) & (r_{\text{BH}} \leq r \leq r_{\text{c2}} \left(\frac{m}{E} \right)) \\ 0 & (r_{\text{c2}} \left(\frac{m}{E} \right) < r \leq \infty) \end{cases} \quad (70)$$

This result has contained all contribution from the parameter region $\sqrt{9/8} \leq m/E$. This is a finite and continuous function of r . This is also differentiable except for $r = r_{\text{c2}}$.

From (41) we obtain

$$G_{\text{IIb}\pm, \text{c}} \left(\frac{m}{E}, r \right) = 2 \times \left(\frac{r}{r_{\text{BH}}} \right)^2 \times \begin{cases} \sqrt{1 - \left(\frac{m}{E} \right)^2} F(r) & (r_{\text{BH}} \leq r \leq r_{\text{c1}} \left(\frac{m}{E} \right)) \\ \left[\sqrt{1 - \left(\frac{m}{E} \right)^2} F - \frac{|r-r_{\text{c1}}|}{r} \sqrt{\left\{ \left(\frac{m}{E} \right)^2 - 1 \right\} \frac{r_{\text{cs}}-r}{r}} \right] & (r_{\text{c1}} \left(\frac{m}{E} \right) < r < r_{\text{cs}} \left(\frac{m}{E} \right)) \\ \sqrt{1 - \left(\frac{m}{E} \right)^2} F(r) & (r_{\text{cs}} \left(\frac{m}{E} \right) \leq r \leq r_{\text{c2}} \left(\frac{m}{E} \right)) \\ 0 & (r_{\text{c2}} \left(\frac{m}{E} \right) < r \leq \infty) \end{cases} \quad (71)$$

for $1 < m/E < \sqrt{9/8}$. This is a finite and continuous function of r , however, is not differentiable at $r = r_{c1}, r_{cs}$ and r_{c2} .

When $m/E = 1$, the function G_I and $G_{Ib\pm,c}$ diverge for the limit $r \rightarrow \infty$ because the particle velocity at the infinite distance v_∞ becomes zero. However this divergence does not crucially affect the effective potential (17) because the integration by E in (18) moderates the divergence and the effective Higgs mass (18) becomes finite for $r \rightarrow \infty$.

6 Dynamical Formation of Spherical Domain Wall

In this section we concretely derive the effective potential for the Higgs vev and consider the wall formation. The effective potential (17) is governed by the effective Higgs mass $\mu_{\text{eff}}^2(r; \mathcal{N})$ defined in (18).

6.1 Effective Higgs Mass around Black Hole

By substituting the particle-density-distribution $\mathcal{N}(E, r)$ resulted in (62), the effective Higgs mass $\mu_{\text{eff}}^2(r; \mathcal{N})$ in (18) becomes

$$\mu_{\text{eff}}^2(r) = -\mu^2 + \frac{1}{8\pi^2} \frac{1}{F(r)} \left(\frac{r_{\text{BH}}}{r}\right)^2 \sum_f g_f Y_f^2 \int_0^\infty dE E f_{T_{\text{BH}}}(E) \frac{1}{2} G\left(\frac{m_f}{E}, r\right). \quad (72)$$

By defining a form function

$$H_f\left(\frac{m_f}{T_{\text{BH}}}, r\right) = \frac{6}{\pi^2} \int_0^\infty ds s f_1(s) \frac{1}{2} G\left(\frac{m_f}{T_{\text{BH}} s}, r\right), \quad (73)$$

we can rewrite

$$\mu_{\text{eff}}^2(r) = -\mu^2 + \frac{1}{48} \frac{1}{F(r)} \left(\frac{r_{\text{BH}}}{r}\right)^2 T_{\text{BH}}^2 \sum_f g_f Y_f^2 H_f\left(\frac{m_f}{T_{\text{BH}}}, r\right). \quad (74)$$

The shapes of the form function (73) are shown in Figure 6. The form function (74) is defined for $r_{\text{BH}} \leq r \leq \infty$. The range of the form function (74) becomes $0 \leq H_f(m/T_{\text{BH}}, r) \leq 27/16$ for bosons and $0 \leq H_f(m/T_{\text{BH}}, r) \leq 27/32$ for fermions.

Non General Relativistic Limit — If we omit the general relativistic (GR) effects as $F(r) = 1$ and $\frac{1}{2}G_f = 1$, we obtain $H_f = 1$ for any boson and $H_f = \frac{1}{2}$ for any fermion. Then the effective Higgs mass becomes

$$\mu_{\text{eff}}^2(r) = -\mu^2 + \frac{A^2}{r^2}, \quad (75)$$

where we have defined *the wall formation constant* as

$$A^2 := \frac{1}{768\pi^2} \sum_f \tilde{g}_f Y_f^2 \quad (76)$$

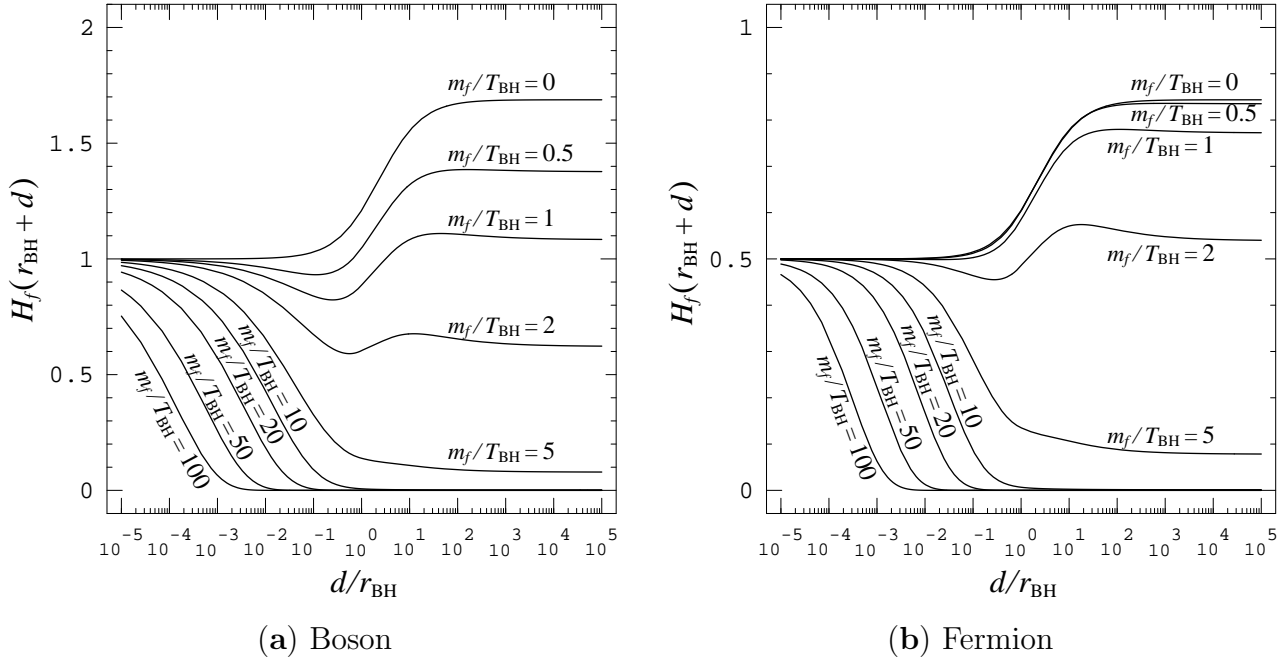


Figure 6: Shapes of the form-function $H_f(\frac{m_f}{T_{\text{BH}}}, r)$ defined in (73) for various m_f/T_{BH} and for (a) bosons and for (b) fermions. The horizontal axis d/r_{BH} is the distance from the horizon $d = r - r_{\text{BH}}$, which is normalized by the Schwarzschild radius r_{BH} . For any m_f/T_{BH} , we have the near-horizon limits $H_f(r \rightarrow r_{\text{BH}}) \rightarrow 1$ for bosons and $H_f(r \rightarrow r_{\text{BH}}) \rightarrow 1/2$ for fermions. For massless particles, we have $H_f(r \rightarrow \infty) \rightarrow 27/16 = 1.6875$ for bosons and $H_f(r \rightarrow \infty) \rightarrow 27/32$ for fermions.

and an effective degree of the freedom as

$$\tilde{g}_f := \begin{cases} g_f & (f : \text{boson}) \\ \frac{1}{2}g_f & (f : \text{fermion}) \end{cases}. \quad (77)$$

The effective Higgs mass (75) reproduces the result in our previous work [8] where the GR effects including the red-shift-effect near the horizon and the gray-body-factor are omitted.

High Temperature Limit — When we consider the high temperature limit $T_{\text{BH}} \gg m_f$, the particles with high energy $E \gg m_f$ dominate, then we can approximate

$$\begin{aligned} \frac{1}{2}G\left(\frac{m_f}{E}, r\right) &\simeq \frac{1}{2}G(0, r) \\ &= \frac{1}{2} \frac{r^2}{r_{\text{BH}}^2} - \frac{1}{4} \frac{r}{r_{\text{BH}}} \left(3 - 2\frac{r}{r_{\text{BH}}}\right) \sqrt{1 + 3\frac{r_{\text{BH}}}{r}}. \end{aligned} \quad (78)$$

We can perform the E -integration in (72) because the function G does not depend on E in the limit. We obtain $H_f(0, r) = \frac{1}{2}G(0, r)$ for bosons and $H_f(0, r) = \frac{1}{4}G(0, r)$ for fermions. The effective Higgs mass (72) becomes

$$\mu_{\text{eff}}^2(r) \simeq -\mu^2 + \frac{1}{F(r)} \frac{A^2}{r^2} \frac{1}{2}G(0, r). \quad (79)$$

We can approximate

$$\mu_{\text{eff}}^2(r) \simeq -\mu^2 + \frac{1}{F(r)} \frac{A^2}{r^2} \times \begin{cases} \frac{27}{16} & (r \gg r_{\text{BH}}) \\ 1 & (r \simeq r_{\text{BH}}) \end{cases} \quad (80)$$

because $\frac{1}{2}G(0, r)$ is the slowly increasing function which takes value from 1 to $\frac{27}{16} = 1.6875$. When we consider the distant region $r \gg r_{\text{BH}}$, our high temperature limit (80) agrees with the non general relativistic limit (75) except for the factor $\frac{27}{16}$. The difference of the factor $\frac{27}{16}$ comes from the difference of the absorption cross sections, namely, the gray body factor makes this difference. When we omit the GR effects for the radiated particle, the absorption cross section is given by the horizon area $4\pi r_{\text{BH}}^2$. On the other hand, the absorption cross section for the massless particle which obeys the Schwarzschild metric becomes $\sigma_{\text{BH}} = \frac{27}{4}\pi r_{\text{BH}}^2$ in (46). When we consider the near-horizon-region, the effective Higgs mass (80) is governed by the factor $1/F(r)$ which diverges on the horizon.

Low Temperature Limit — When we consider the black hole with the low Hawking temperature limit $T_{\text{BH}} \ll m_f$, we can approximate

$$\frac{1}{2}G \simeq \frac{1}{2}G_{\text{Iib}} = \begin{cases} \left(\frac{r}{r_{\text{BH}}}\right)^2 \sqrt{1 - \left(\frac{m_f}{E}\right)^2 F(r)} & (r_{\text{BH}} \leq r \leq r_{c2}\left(\frac{m_f}{E}\right)) \\ 0 & (r_{c2}\left(\frac{m_f}{E}\right) < r \leq \infty) \end{cases}. \quad (81)$$

Then the effective Higgs mass (72) becomes

$$\mu_{\text{eff}}^2(r) \simeq -\mu^2 + \frac{1}{8\pi^2} \frac{1}{F(r)} T_{\text{BH}}^2 \sum_f g_f Y_f^2 \int_{\frac{m_f \sqrt{F(r)}}{T_{\text{BH}}}}^{\infty} ds f_1(s) \sqrt{s^2 - \frac{m_f^2 F(r)}{T_{\text{BH}}^2}}. \quad (82)$$

When we consider the distant region $r \gg r_{c2}(\frac{m_f}{T_{\text{BH}}})$ where the particle with the energy $E \approx T_{\text{BH}}$ cannot reach, the only high-energy-side of the tails of the distribution $f_{T_{\text{BH}}}(E)$ contributes to (72). The difference between boson and fermion is negligible for (82) in the distant region because the high energy tails of the distribution $f_{T_{\text{BH}}}(E)$ for bosons and for fermions are almost the same. Therefore we can adopt the Maxwell distribution to evaluate (82) in the distant region instead of the Fermi-Dirac or the Bose-Einstein distribution. By using the Maxwell distribution $f_{T_{\text{BH}}}(E) = \exp(-E/T_{\text{BH}})$, we can perform the integration and obtain

$$\mu_{\text{eff}}^2(r) \simeq -\mu^2 + \frac{1}{8\pi^2} \frac{1}{F(r)} T_{\text{BH}}^2 \sum_f g_f Y_f^2 \frac{m_f \sqrt{F}}{T_{\text{BH}}} K_1 \left(\frac{m_f \sqrt{F}}{T_{\text{BH}}} \right) \quad (83)$$

where K_1 is the modified Bessel function of the second kind. On the other hand, when we consider the near horizon region $r_{\text{BH}} < r < r_{c2}(\frac{m_f}{T_{\text{BH}}})$, we can approximate

$$\mu_{\text{eff}}^2(r) \simeq -\mu^2 + \frac{1}{48} \frac{1}{F(r)} T_{\text{BH}}^2 \sum_f \tilde{g}_f(r) Y_f^2, \quad (84)$$

where we have defined *the local effective degree of the freedom* as

$$\tilde{g}_f(r) := \begin{cases} g \times \exp \left[-0.60\sqrt{2}\sqrt{F(r)}\frac{m_f}{T_{\text{BH}}} \right] & (\text{boson}) \\ \frac{1}{2}g \times \exp \left[-\left(0.39\sqrt{2}\sqrt{F(r)}\frac{m_f}{T_{\text{BH}}}\right)^{3/2} \right] & (\text{fermion}) \end{cases}. \quad (85)$$

The only the radiated particle which can reach the position r contributes to the local effective degree of the freedom $\tilde{g}_f(r)$ on the position r .

Summarized Form — Finally we can summarize the approximated effective Higgs mass for all parameter regions as

$$\mu_{\text{eff}}^2(r) \simeq -\mu^2 + \frac{1}{F(r)} \frac{A(r)^2}{r^2}, \quad (86)$$

where we have defined *the local wall formation parameter* $A(r)$ as the same way of (76) by using the local effective degree of the freedom $\tilde{g}_f(r)$ in (85) instead of \tilde{g}_f in (77). As compared with the exact form (74), the approximated form (86) contains an error of the factor one. By defining *the local Hawking temperature* as

$$\tilde{T}_{\text{BH}}(r) := \frac{T_{\text{BH}}}{\sqrt{F(r)}}, \quad (87)$$

we can approximate the local effective degree of the freedom (85) as follows

$$\tilde{g}_f(r) \simeq \begin{cases} \tilde{g}_f & \left(\tilde{T}_{\text{BH}}(r) \gtrsim m_f \right) \\ 0 & \left(\tilde{T}_{\text{BH}}(r) \lesssim m_f \right) \end{cases}. \quad (88)$$

This property is very similar to the temperature-dependency of the degree of freedom in the relativistic thermodynamics. We present a energy-density-distribution $\rho(r)$ near the horizon as $\rho(r) \simeq \frac{\pi^2}{30} g_{*f}(\tilde{T}_{\text{BH}}(r)) \tilde{T}_{\text{BH}}^4(r)$ in Appendix B. This energy-density-distribution reproduces the relativistic thermodynamical relation with the temperature $T = \tilde{T}_{\text{BH}}(r)$. The region near the horizon is not thermal equilibrium which is required for thermodynamical treatments, however, several behaviors near the horizon are very similar to that of the thermal equilibrium with the local Hawking temperature $\tilde{T}_{\text{BH}}(r)$.

6.2 Wall Structure Solutions

By substituting the resultant effective Higgs mass (86), the effective potential (17) becomes

$$V_{\text{eff}}(\phi, r) = \frac{1}{2} \left[-\mu^2 + \frac{1}{F(r)} \frac{A^2(r)}{r^2} \right] \phi^2 + \frac{1}{2} \frac{\mu^2}{v^2} \phi^4. \quad (89)$$

The equation for the Higgs vev in (15) with the effective potential (89) becomes

$$\frac{1}{r^2} \partial_r (r^2 F(r) \partial_r \phi) = \frac{1}{2} \left(-\mu^2 + \frac{1}{F(r)} \frac{A(r)^2}{r^2} \right) \phi + \frac{\mu^2}{v^2} \phi^3. \quad (90)$$

The factor $1/F(r)$ in both the effective potential (89) and the field equation (90) always diverges on the horizon. The form of the effective potential (89) near the horizon is different from that in the distant region (see Figure 7). The minimum of the effective potential $V_{\text{eff}}(\phi, r)$ in (89) depends on the position r . The effective potential $V_{\text{eff}}(\phi, r)$ is minimized by $\phi = 0$ near the horizon because the sign of $\mu_{\text{eff}}^2(r)$ in (86) inverts when the position r approach the horizon. Therefore we expect the formation of the spherical wall-structure of the Higgs vev around the horizon even if $T_{\text{BH}} < \mu$. It is difficult to define the exact radius of the wall-structure because the Higgs vev is continuously varying in the wall-structure. However we can define *the characteristic wall radius* r_{DW} by

$$\mu_{\text{eff}}(r_{\text{DW}}) = 0, \quad (91)$$

as a typical scale of the wall-radius. On the radius the sign of $\mu_{\text{eff}}^2(r)$ inverts.

To simplify the analysis of the wall structure we assume that the wall formation parameter A^2 is a constant. The characteristic wall radius becomes

$$r_{\text{DW}} = \frac{1}{2} \left[r_{\text{BH}} + \sqrt{r_{\text{BH}}^2 + \frac{A^2}{\mu^2}} \right] \quad (92)$$

as one of the solutions of the equation (91). The effective potential (89) is minimized at each point by the value of the Higgs field:

$$\phi_{\text{min}}(r) = \begin{cases} \frac{v}{\sqrt{2}} \left[1 - \frac{F(r_{\text{DW}}) r_{\text{DW}}^2}{F(r) r^2} \right]^{1/2} & (r \geq r_{\text{DW}}) \\ 0 & (r < r_{\text{DW}}) \end{cases} \quad (93)$$

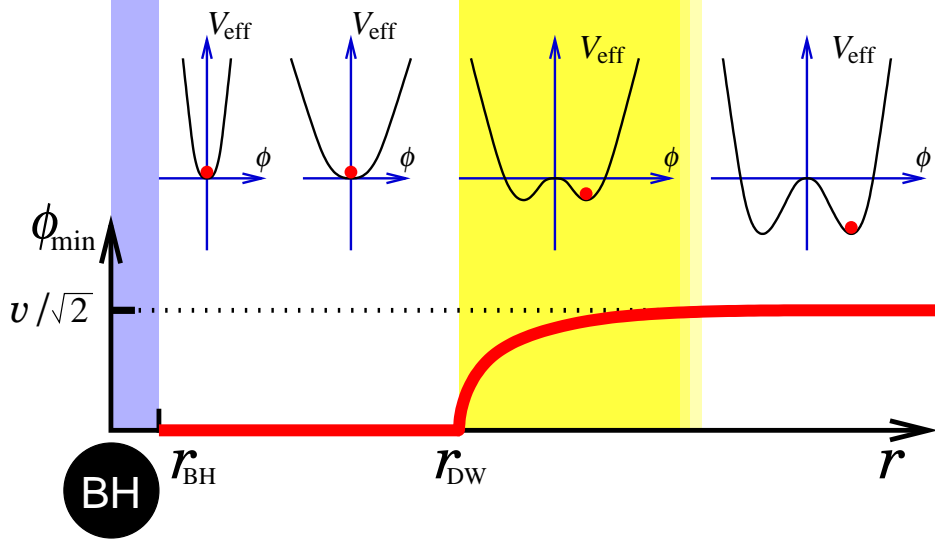


Figure 7: Function-forms of the effective Higgs potential $V_{\text{eff}}(\phi, r)$ which is depending on the distance from the black hole. The dot in the potential-curve means the minimum of the potential at each r . The thick curve is the distribution of the Higgs field $\phi_{\text{min}}(r)$ which minimizes the effective potential $V_{\text{eff}}(\phi, r)$ at each r .

The form of $\phi_{\text{min}}(r)$ is shown in Figure 8 for various values of $d_{\text{DW}}/r_{\text{BH}}$. The normalized form of $\phi_{\text{min}}(r)$ is determined by $d_{\text{DW}}/r_{\text{BH}}$.

The physical phenomena outside of the horizon are considered and the inside of the horizon is not relevant to our subject. To clarify this we introduce a new positive coordinate d instead of r as a distance from the horizon:

$$r = r_{\text{BH}} + d. \quad (94)$$

We also define a characteristic-wall-distance d_{DW} instead of the characteristic-wall-radius r_{BH} , which satisfies

$$r_{\text{DW}} = r_{\text{BH}} + d_{\text{DW}}. \quad (95)$$

We introduce a profile function of the Higgs vev as

$$f(s) := \frac{1}{v/\sqrt{2}} \phi(r_{\text{BH}} + d_{\text{DW}} s), \quad (96)$$

which is dimensionless function and has value $f = 1$ in the ordinary vacuum. The parameter s is a distance from horizon normalized by d_{DW} . The equation of the Higgs vev (90) becomes

$$\frac{1}{(s_0 + s)^2} \frac{\partial}{\partial s} \left[(s_0 + s)s \frac{\partial}{\partial s} f \right] = \frac{A^2}{2} \frac{1}{(s_0 + 1)} \left[\left\{ -1 + \frac{(s_0 + 1)}{(s_0 + s)s} \right\} f + f^3 \right], \quad (97)$$

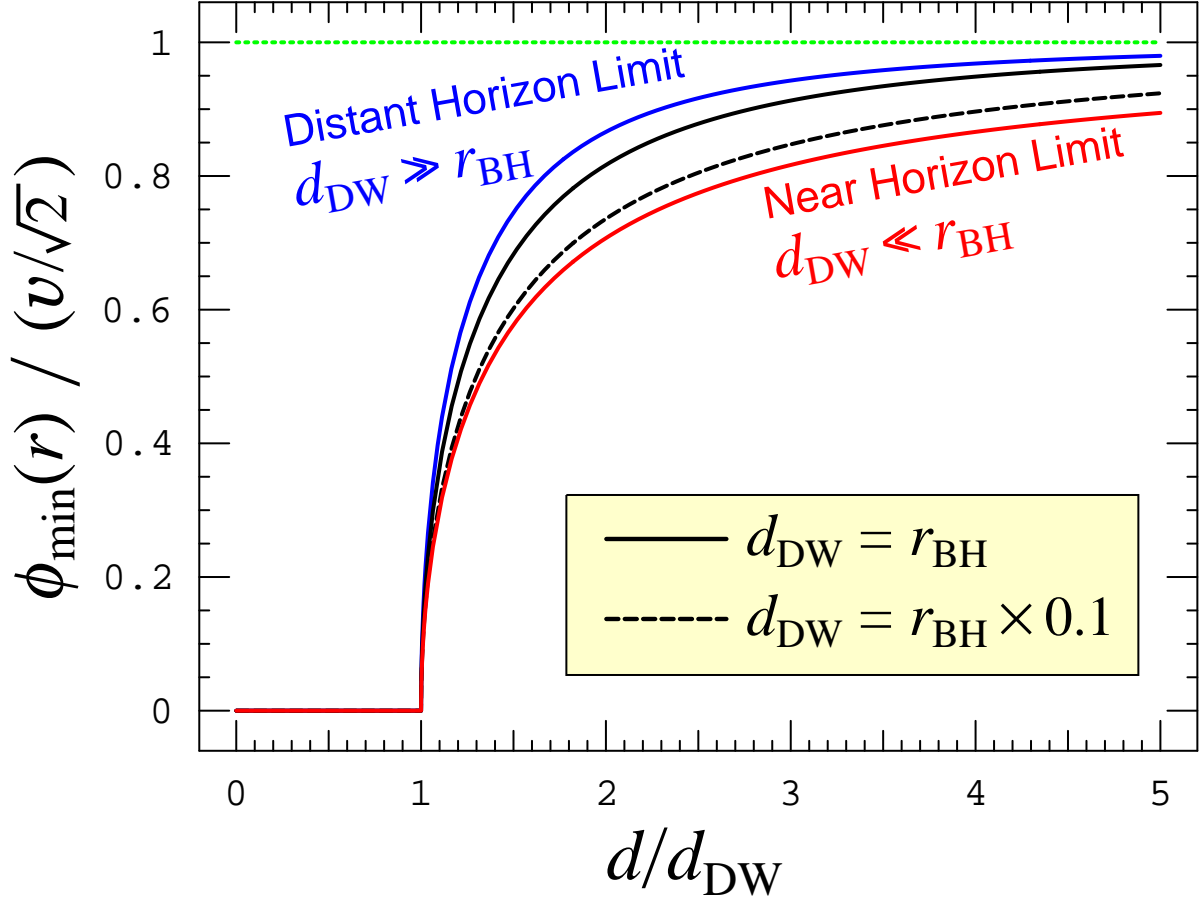


Figure 8: Distributions of the Higgs field $\phi_{\min}(r)$ which minimizes the effective potential $V_{\text{eff}}(\phi, r)$ at each point. The horizontal axis is the distance from the horizon d normalized by the characteristic-wall-distance d_{DW} . (We note the relations $r = r_{\text{BH}} + d$ and $r_{\text{DW}} = r_{\text{BH}} + d_{\text{DW}}$.) The dotted line $\phi = v/\sqrt{2}$ is the ordinary Higgs vev and the vertical axis is normalized by $v/\sqrt{2}$. The form of $\phi_{\min}(r)$ is depending on the ratio $d_{\text{DW}}/r_{\text{BH}}$. The uppermost curve describes $\phi_{\min}(r)$ in the distant horizon limit $d_{\text{DW}} \rightarrow \infty$ with keeping r_{BH} constant. The lowest curve describes $\phi_{\min}(r)$ in the near horizon limit $d_{\text{DW}} \rightarrow 0$ with keeping r_{BH} constant.

where we have defined a ratio $s_0 := r_{\text{BH}}/d_{\text{DW}}$. This differential equation for the profile function is depending on both the ratio s_0 and the wall-formation constant A^2 .

To determine the Higgs vev structure around the black hole by the differential equation (97), we should consider the boundary conditions. In the ordinary vacuum, the Higgs vev is $\phi = v/\sqrt{2}$ which is given by the minimum of the bare Higgs potential (4). The resultant effective potential $V_{\text{eff}}(\phi, r)$ in (89) agrees with the bare potential (4) for $r \rightarrow \infty$. Then the boundary condition

$$(a) \quad \phi(r) \rightarrow v/\sqrt{2} \text{ for } r \rightarrow \infty$$

is required. This condition is equivalent to a condition $f(s) \rightarrow 1$ for $s \rightarrow \infty$. If there is no Hawking radiation, we expect that nothing special about the Higgs vev happens on the horizon. When we turn on the Hawking radiation, we expect a finite deformation of the Higgs vev around and on the horizon. Therefore the boundary condition

$$(b) \quad \phi(r) \text{ is finite on the horizon } r = r_{\text{BH}}$$

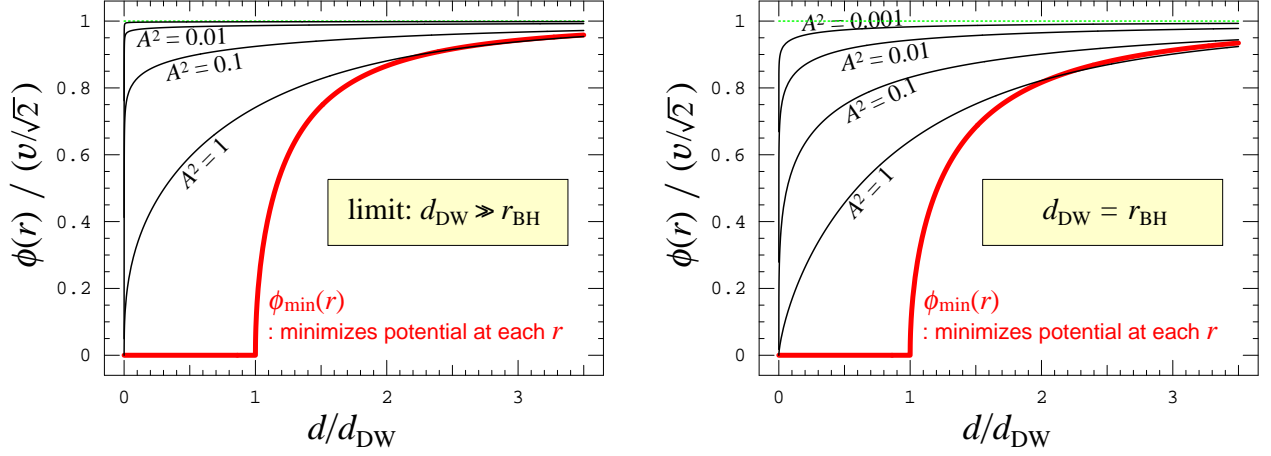
is also required. This is equivalent to the finiteness of the profile function $f(s)$ on $s = 0$.

Provided that the length-ratio $s_0 = r_{\text{BH}}/d_{\text{DW}}$ and the wall formation constant A^2 are given, the solution of the differential equation (97), which satisfies the boundary conditions (a) and (b), is uniquely determined. In the Appendix C we consider the solutions near the horizon ($d \ll d_{\text{DW}}$) analytically. The near-horizon-solution which satisfy the boundary condition (b) is given by

$$f(s) = C_+ s^{+\sqrt{\frac{A^2}{2}}} \times {}_2F_1 \left[\frac{1}{2} + \sqrt{\frac{A^2}{2}} - \sqrt{\frac{1}{4} + \frac{A^2}{2}}, \frac{1}{2} + \sqrt{\frac{A^2}{2}} + \sqrt{\frac{1}{4} + \frac{A^2}{2}}; 1 + 2\sqrt{\frac{A^2}{2}}; -\frac{s}{s_0} \right], \quad (98)$$

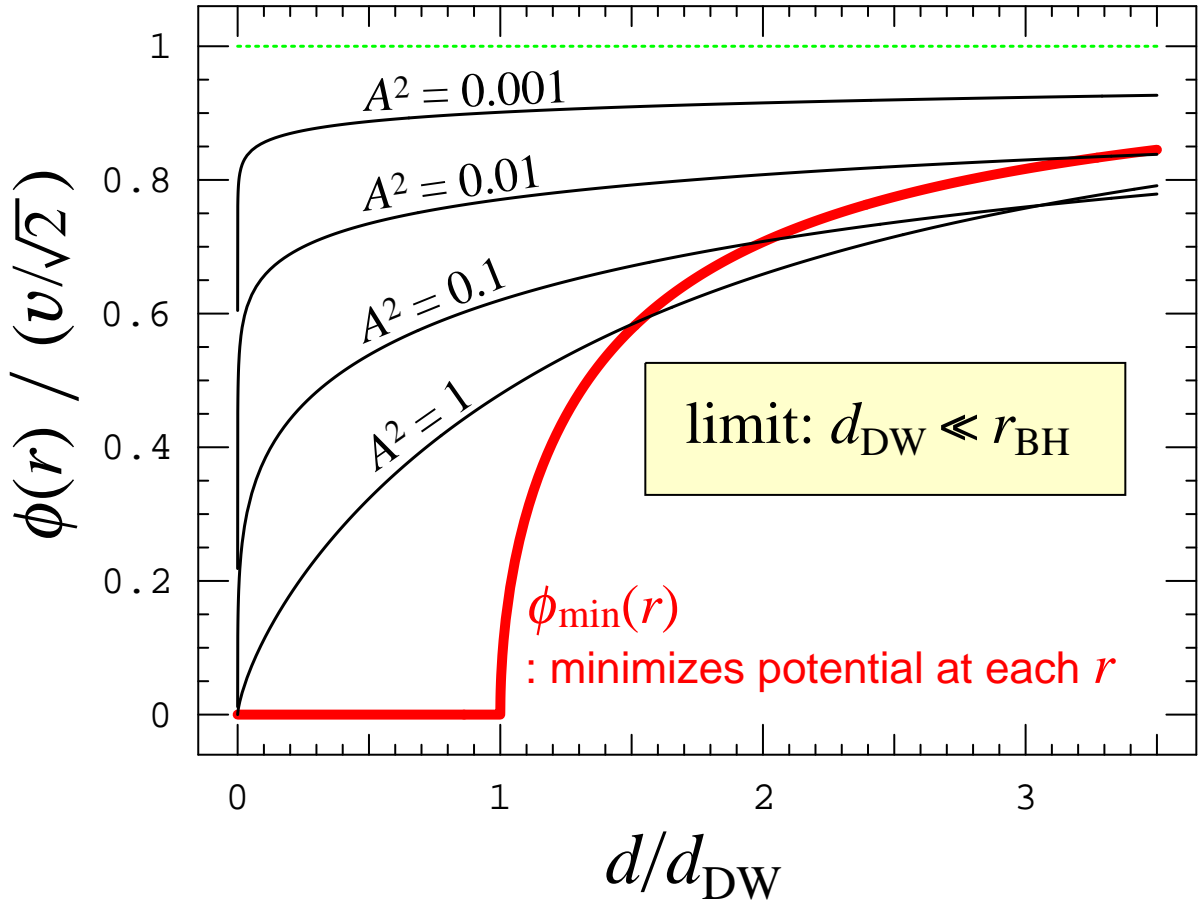
where C_+ is a positive constant and ${}_2F_1$ is the hypergeometric function. This solution is defined for $s \geq 0$. The near-horizon-solution (98) is a monochromatic increasing function and has property $f(s) \rightarrow 0$ for $s \rightarrow 0$. We can numerically solve the equation (97) so that the numerical solution is a numerical extrapolation of the near-horizon-solution (98). The value of the constant C_+ should be so chosen that the numerical solution satisfies the boundary condition (a). Namely, the constant C_+ is determined by the matching for the near-horizon-solution and the numerical solutions. The numerical solutions for various value of both the parameters $r_{\text{BH}}/d_{\text{DW}}$ and A^2 are shown in Figure 9.

The limit $d_{\text{DW}} \gg r_{\text{BH}}$ in Figure 9 (a) is corresponding to the limit $T_{\text{BH}} \gg \mu$, because of both the relation $d_{\text{DW}} \simeq r_{\text{DW}} \simeq A/\mu$ in this limit and the relation $T_{\text{BH}} = \frac{1}{4\pi} \frac{1}{r_{\text{BH}}}$. In this limit the Hawking temperature T_{BH} is much greater than the critical temperature ($\sim \mu$) of the phase transition of the Higgs field. The numerical result shown in Figure 9 (a) indicates the formation of the wall-structure of the Higgs vev. The general relativistic effects are negligible



(a) Wall with distant-horizon-limit

(b) Comparable case of $d_{\text{DW}} = r_{\text{BH}}$



(c) Wall with near-horizon-limit

Figure 9: Resultant structures of the Higgs vev around the black hole. (a) A wall with distant-horizon-limit ($d_{\text{DW}} \gg r_{\text{BH}}$), (b) a comparable case $d_{\text{DW}} = r_{\text{BH}}$ and (c) a wall with near-horizon-limit ($d_{\text{DW}} \ll r_{\text{BH}}$) are shown. For each figure the solutions for $A^2 = 0.001, 0.01, 0.1$ and 1 are shown as thin curves. The thick curves $\phi_{\text{min}}(r)$ are the Higgs fields which minimize the effective potential at each point.

because the formed wall-structure is much distant from the horizon. This result reproduces the wall-structure concluded in our previous work [8] where the general relativistic effects are omitted.

When we consider a comparable case $d_{\text{DW}} = r_{\text{BH}}$ in Figure 9 (b), the Hawking temperature T_{BH} and the critical temperature ($\sim \mu$) of the gauge-Higgs-Yukawa theory are also comparable. We also find the wall-structure around the black hole in the same way. The Higgs vev vanishes on the horizon: $\phi(r_{\text{BH}}) = 0$, then the symmetry which has been spontaneously broken down by the bare Higgs potential (4) is restored on the horizon. Therefore the wall separates the symmetric phase region on the horizon from the background of the broken phase vacuum $\phi = v/\sqrt{2}$. The restoration of the symmetry on the horizon is essentially caused by the general relativistic effect of the Hawking-radiated particles.

The wall-structure for the near-horizon-limit $d_{\text{DW}} \ll r_{\text{BH}}$ shown in Figure 9 (c) is more interesting. This limit is corresponding to the limit $T_{\text{BH}} \ll \mu$, namely, the Hawking temperature is much lower than the critical temperature ($\sim \mu$) of the phase transition of the gauge-Higgs-Yukawa theory. In the previous work [8] where the general relativistic effects are omitted, we concluded that such a cold black hole cannot form the wall-structure by the Hawking radiation. However the general relativistic effects of the Hawking radiation form the wall-structure shown in Figure 9 (c) and restore the spontaneously-broken-symmetry on the horizon. The characteristic-wall-distance in this limit becomes

$$d_{\text{DW}} \simeq \frac{A^2}{4} \frac{1}{r_{\text{BH}} \mu^2}. \quad (99)$$

Finally, we conclude that the Hawking radiation of a black hole forms a spherical domain wall around the black hole even if the Hawking temperature is much smaller than the critical temperature of the phase transition.

7 CONCLUSION AND DISCUSSIONS

In this paper we have proposed a general relativistic (GR) formulation of the ballistic model to consider the Hawking radiation from the Schwarzschild black hole in the vacuum of the gauge-Higgs-Yukawa theory. We have found that the wall-structure of the Higgs scalar vev is formed even if the Hawking temperature is smaller than the energy scale of the gauge-Higgs-Yukawa theory. In the previous work where the GR effects were not considered, the critical Hawking-temperature for the wall-formation was found out [8], however, we find out the absence of the critical Hawking-temperature. When the Hawking temperature T_{BH} is much smaller than the energy scale of the field theory $\sim \mu$, we find the wall-structure closely near the horizon. The approximated width of the wall-structure near the horizon becomes the characteristic-wall-distance in (99). On the horizon we also find the restoration of the

symmetry which has been spontaneously broken down by the bare Higgs potential (4). These results are essentially produced by the GR effects on the Hawking-radiated particles and on the Higgs field.

Here we discuss validity of the GR formulation of the ballistic model. The ballistic model is valid when (a) the mean free path of the radiated particles is longer than the length-scale of the wall-structure d_{DW} and (b) the mean wavelength of the radiation is shorter than the length-scale d_{DW} . The condition (a) is satisfied when the Hawking temperature T_{BH} is smaller than the critical Hawking temperature of the thermalization T_{BH}^* which is much greater than the critical temperature of the gauge-Higgs-Yukawa theory ($\sim \mu$). When T_{BH} is greater than T_{BH}^* , the wall-structure by the thermal phase transition rather than our mechanism is formed. This can be confirmed by considering the interaction-rates around the black hole [4, 5]. The mean wavelength of the radiated particles is approximately given by the Schwarzschild radius r_{BH} for the region distant from the horizon, where the GR effects for the radiation are negligible. When we consider a situation $T_{\text{BH}} \gtrsim \mu$, the wall-structure distant from the horizon ($d_{\text{DW}} \gtrsim r_{\text{BH}}$) is formed and the condition (b) is satisfied. On the other hand, when we consider a situation $T_{\text{BH}} \lesssim \mu$, the wall-structure near the horizon ($d_{\text{DW}} \lesssim r_{\text{BH}}$) is formed and the GR effects become important. The mean wavelength near the horizon becomes short by the red-shift effect. Parikh and Wilczek showed that the Hawking radiation can be regard as the quantum-tunneling of the particle through the horizon [7]. They employed a particle description, which is very similar to our ballistic model, and the correct spectrum of the Hawking radiation is reproduced. In their argument the particle description near the horizon becomes valid because of the red-shift effect. Then we also expect that our ballistic description is valid not only for the distant-horizon but also for the near-horizon.

In our GR formulation of the ballistic model, the Higgs scalar vev around the black hole is determined by the effective potential $V_{\text{eff}}(\phi, r; \mathcal{N})$ in (16) which is depending on a density-distribution $\mathcal{N}_f(E, r)$ of both the particle-position r and the particle-energy E . The symmetry-restoration on the horizon and the wall formation near the horizon are essentially caused by the divergence of the density-distribution $\mathcal{N}_f(E, r)$ on the horizon. The density-distribution $\mathcal{N}_f(E, r)$ is depending on the particle-flux $f_f(E, \omega)$ on the horizon, which is the distribution of the initial radiation-zenith-angle ω and of the particle-energy E (see Figure 2). The divergence on the horizon of the distribution $\mathcal{N}_f(E, r)$ is caused by the $\cos^{-3} \omega$ factor of the resultant flux $f_f(E, \omega)$ in (51). The flux $f_f(E, \omega)$ on the horizon is quite different from that for the normal black-body-radiation (52) which includes the factor $\cos \omega$. Therefore domination of the low elevation-angle (i.e., high initial radiation-zenith-angle $\omega \sim \pi/2$) on the horizon plays important role in the wall-formation near the horizon.

Here we summarize the derivation of the flux (51) with low elevation-angle domination.

The flux (51) is derived by an analytic continuation of the flux defined for high elevation-angle-region $0 \leq \omega < \omega_c$ into the flux for all elevation-angle $0 \leq \omega < \pi/2$. The flux for the high elevation-angle $0 \leq \omega < \omega_c$ is calculated by the two assumptions; (i) the motion of the particles radiated from the horizon is determined by the geodesic on the Schwarzschild space-time and (ii) the observer at the infinite distance finds a disk-image with *uniform intensity* of the black-body-radiation for each particle-energy as the image of the radiated particles. The assumption (i) is the simplest application of the general relativity to the Hawking-radiated particles. The assumption (ii) may be valid because the observation of the image with non-uniform strength means that the Hawking radiation is not thermal radiation and carries out some information from the black hole.

The domination of the radiation with low elevation-angle is consistent with the picture of the heat-bath around the horizon with the local Hawking temperature $T_{\text{BH}}(r) \simeq T_{\text{BH}}/\sqrt{F(r)}$ (see Appendix A). The energy-density-distribution of the Hawking radiation $\rho(r)$, which is derived from the resultant particle-density-distribution $\mathcal{N}_f(E, r)$ in (62), is also consistent with $T_{\text{BH}}(r)$ (see Appendix B). We have pointed out that $T_{\text{BH}}(r)$ naturally arises in the resultant effective Higgs mass in (86). Hotta discussed that the temperature closely near the horizon becomes very high due to the picture of the heat-bath with the local temperature $T_{\text{BH}}(r)$ and the thermal phase transition in the string theory arises [14].

The total energy of the Hawking-radiated particle between the sphere near the horizon with a radius $r_{\text{BH}} + d$ and the distant sphere with a radius R is given by

$$E_{\text{total}}(d, R) := \int_{r_{\text{BH}}+d}^R 4\pi r^2 dr \rho(r). \quad (100)$$

This total energy should be finite, however, this has an IR divergence for $R \rightarrow \infty$ and an UV divergence for $d \rightarrow 0$. Because the black hole has a finite lifetime τ_{BH} , there arises a natural IR cut-off for the radius $R_{\text{cutoff}} \sim \tau_{\text{BH}}$. Then the IR divergence is easily solved. On the other hand, the UV divergence $E_{\text{total}} \sim 1/d$ is an open problem. A cut-off of the Hawking radiation near the horizon may be required. This cut-off is equivalent to the cut-off for low elevation-angle domination, namely, the analytic continuation is restricted to $0 < \omega < \pi/2 - \varepsilon$ with finite ε . This problem may be solved by quantum gravity, then the cut-off may be given by the Planck length scale $d_{\text{cutoff}} \sim l_{\text{pl}}$. If we take the cut-off in the Planck length scale, our argument in this paper is valid for $d > l_{\text{pl}}$. Therefore we expect that our results are valid as long as we consider low energy ($\ll m_{\text{pl}}$) phase transition. Hotta discussed that the cut-off is given by $T_{\text{BH}}(r_{\text{cutoff}}) \sim m_{\text{pl}}$ and all of energy and all of the information (entropy) are carried by the Hawking radiation, i.e., $E_{\text{total}} = m_{\text{BH}}$ [14]. In this case, the cut-off r_{cutoff} is much smaller than the Planck length l_{pl} .

Finally we discuss applications of the wall-structure. We expect a net charge-transportation into the black hole by the Hawking radiation and a phenomenon of the spontaneous charge-up

of the black hole by the effect of the wall-structure [8]. We also expect the baryon number production [11] by the transportation of the hyper charge [12, 13]. This production-mechanism may be realized by the thin-wall black-hole baryogenesis or the direct black-hole baryogenesis proposed in [6].

The wall-formation near the horizon is caused by the Hawking-radiated particles with low elevation-angle. All of such particles return into the horizon and are not directly observed by the observer at the infinity distance. One may consider that the radiation with low elevation-angle and the wall-formation near the horizon belong to a metaphysical subject. However the formation of the wall-structure near the horizon can be confirmed by the observation of the net charge flux from the black hole. Therefore the wall-formation near the horizon is not metaphysical.

ACKNOWLEDGMENTS

I would like to thank Ofer Aharony, Micha Berkooz, Alex Buchel, Hikaru Kawai, Barak Kol, Joan Simon and Leonard Susskind for useful discussions. I am grateful to K. Shigetomi for helpful advice and also for careful reading of the manuscript. The work has been supported by the Koshland Postdoctoral Fellowship of the Weizmann Institute of Science.

APPENDIX A: Radiation Angle Distribution and Metric

In this appendix we show that the radiation-angle-dependency of the the Hawking radiation on the horizon (the factor $1/\cos^3 \omega$ in (51)) is naturally derived from the property of the space-time. Around the black hole described by the Schwarzschild metric (2), a short line-element dr near the horizon in the Schwarzschild coordinate system becomes a long line-element

$$ds_r = \frac{1}{\sqrt{F}} dr. \quad (101)$$

in the proper coordinate system. Namely the Schwarzschild coordinate system compress the r -direction near the horizon (see Figure 10). This compression changes the zenith-angle near the horizon. The zenith-angle of a line-element in the the Schwarzschild coordinate system (the thick segment in Figure 10 (B)) is defined as

$$\tan \omega = \frac{rd\theta}{dr} \quad (102)$$

which is used for the radiation-zenith-angle in the main part of this paper. On the other hand, the zenith-angle of the same line-element in the proper coordinate system (the thick

segment in Figure 10 (A)) becomes

$$\tan \varphi = \frac{rd\theta}{ds_r}. \quad (103)$$

These zenith-angles ω and φ are different description of the same line-element, then a relation between these angles is derived from the definitions (102), (103) and the relation (101) as

$$\tan \varphi = \sqrt{F} \tan \omega. \quad (104)$$

For convenience we define a function

$$A(F, \omega) := 1 + \left(\frac{1}{F} - 1 \right) \cos^2 \omega, \quad (105)$$

then we obtain several relations

$$\frac{\partial \phi}{\partial \omega} = \frac{1}{\sqrt{F}} \frac{1}{A(F, \omega)}, \quad (106)$$

$$\cos^2 \phi = \frac{1}{F} \frac{\cos^2 \omega}{A(F, \omega)}, \quad (107)$$

$$\sin^2 \phi = \frac{\sin^2 \omega}{A(F, \omega)}. \quad (108)$$

We put a angle-distribution of particle-flux on the φ -coordinate system as

$$d\mathcal{F} = \tilde{f}(E, \varphi) \times dE \times d\varphi \sin \varphi d\psi. \quad (109)$$

The angle-distribution (109) can be rewritten for the ω -coordinate system as

$$\begin{aligned} d\mathcal{F} &= \tilde{f}(E, \varphi(\omega)) \frac{d\varphi \sin \varphi(\omega)}{d\omega \sin \omega} \times dE \times d\omega \sin \omega d\psi \\ &\equiv f(E, \omega) \times dE \times d\omega \sin \omega d\psi, \end{aligned} \quad (110)$$

then we obtain the relation

$$f(E, \omega) = \tilde{f}(E, \varphi(\omega)) \frac{1}{F^{1/2} A(F, \omega)^{3/2}}, \quad (111)$$

which gives us the coordinate transformation law ($\omega \leftrightarrow \varphi$) for the angle-distribution.

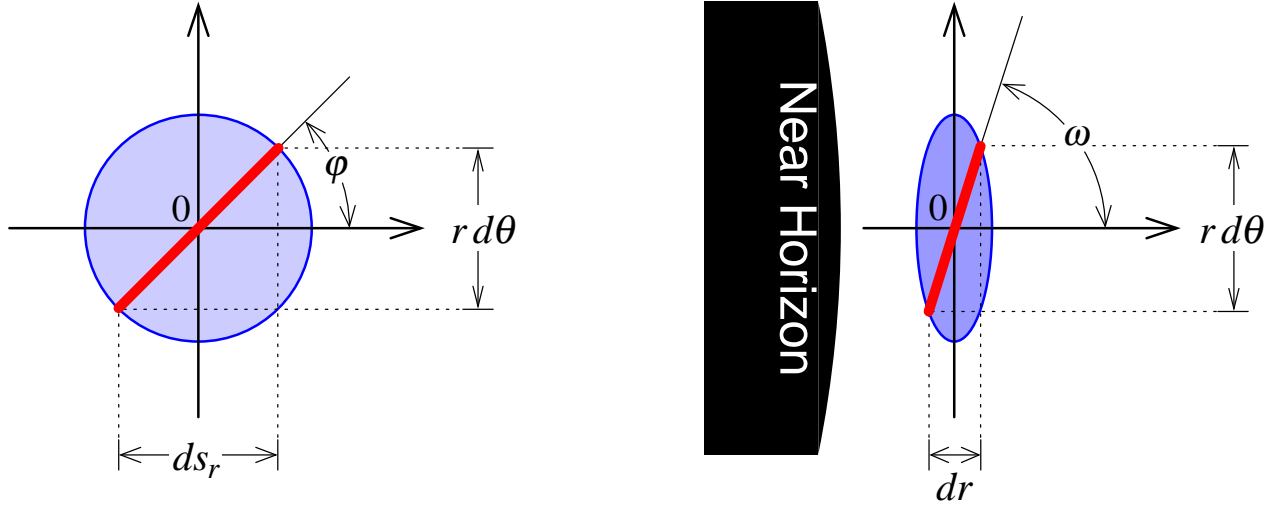
When we consider the near-horizon-limit $r \rightarrow r_{\text{BH}}$, we have $F(r) \rightarrow 0$ and the coordinate transformation for the zenith-angles (104) becomes

$$\varphi(\omega) \rightarrow \begin{cases} 0 & (0 \leq \omega \lesssim \pi/2) \\ \pi/2 & (\omega = \pi/2) \end{cases}. \quad (112)$$

We also obtain the following forms in the limit:

$$A(F, \omega) \rightarrow \frac{1}{F} \cos^2 \omega, \quad (113)$$

$$f(E, \omega) \rightarrow \tilde{f}(E, \varphi(\omega)) \frac{F}{\cos^3 \omega}. \quad (114)$$



(A) Proper Length Element and Angle (B) Coordinate Length Element and Angle

Figure 10: (A) A line-element in the proper-length coordinate system (thick line segment) and (B) the corresponding line-element in the Schwarzschild coordinate system near the horizon (thick line segment). The relation between the coordinate line-elements is $ds_r = F^{-1/2} dr$. The definitions of the zenith-angles of the line-element are $\tan \varphi = rd\theta/ds_r$ and $\tan \omega = rd\theta/dr$. Then we have the relation $\tan \varphi = \sqrt{F} \tan \omega$.

If we assume that the zenith-angle-distribution of the flux $\tilde{f}(E, \varphi)$ in the proper coordinate system is smooth around $\varphi = 0$, we have

$$f(E, \omega) = \tilde{f}(E, 0) \frac{F}{\cos^3 \omega}. \quad (115)$$

in the near-horizon-limit. Here we find another derivation of the factor $1/\cos^3 \omega$ in the angle-distribution of the particle-flux (115). In Section 4 we have derived the distribution of the particle-flux of the Hawking radiation in (51) including the factor $1/\cos^3 \omega$ by analytic continuation and uniformity of the Hawking radiation. On the other hand, the factor $1/\cos^3 \omega$ is derived from the smoothness of the distribution and geometry of the black hole in this appendix.

Inversely if we assume the resultant flux (51), we obtain the flux on the proper coordinate system as

$$\begin{aligned} \tilde{f}_f(E, 0) &= \frac{1}{16\pi} \frac{1}{F} \times g_f f_{T_{\text{BH}}}(E) 4\pi E^2 \\ &= \frac{1}{4\pi} \times g_f \tilde{f}_{\tilde{T}_{\text{BH}}}(\tilde{E}) 4\pi \tilde{E}^2, \end{aligned} \quad (116)$$

where we have defined the proper energy of the particle $\tilde{E}(r) := E/\sqrt{2F(r)}$ and the effective local Hawking temperature $\tilde{T}_{\text{BH}}(r) := T_{\text{BH}}/\sqrt{2F(r)}$. The proper flux for the zenith-direction

$\varphi \simeq 0$ resulted in (116) is consistent with the heat-bath picture with the local Hawking temperature $\tilde{T}_{\text{BH}}(r)$.

APPENDIX B: Energy Density Distribution around the Black Hole

In this appendix we calculate the energy density of the Hawking-radiated particles around the black hole to clarify the physical meaning of our resultant particle number-distribution $N_f(E, r)$ in (62). The energy density of the Hawking-radiated particle at the position r with the particle-species f is given by

$$\rho_f(r) = \int_0^\infty dE E \mathcal{N}_f(E, r). \quad (117)$$

By defining the form function

$$K_f\left(\frac{m_f}{T_{\text{BH}}}, r\right) := \frac{15}{\pi^4} \int_0^\infty ds s^3 f_1(s) \frac{1}{2} G\left(\frac{m_f}{T_{\text{BH}}} \frac{1}{s}, r\right), \quad (118)$$

we obtain

$$\rho_f(r) = \frac{\pi^2}{120} g_f T_{\text{BH}}^4 \times \frac{1}{F^2(r)} \left(\frac{r_{\text{BH}}}{r}\right)^2 K_f\left(\frac{m_f}{T_{\text{BH}}}, r\right). \quad (119)$$

We display the shapes of the form function $K_f(r)$ in Figure 11. For any m_f/T_{BH} , we have the same near-horizon limits $K_f(r \rightarrow r_{\text{BH}}) \rightarrow 1$ for bosons and $K_f(r \rightarrow r_{\text{BH}}) \rightarrow 7/8$ for fermions. For the massless particle we have $K_f(r \rightarrow \infty) \rightarrow \frac{27}{16} \simeq 1.69$ for bosons and $K_f(r \rightarrow \infty) \rightarrow \frac{27}{32} \times \frac{7}{8} \simeq 1.48$ for fermions.

The energy-density (119) has an interesting approximated form:

$$\rho_f(r) \simeq \frac{\pi^2}{30} g_{*f}(\tilde{T}_{\text{BH}}(r)) \tilde{T}_{\text{BH}}^4(r) \times \left(\frac{r_{\text{BH}}}{r}\right)^2, \quad (120)$$

where we have defined the local Hawking temperature

$$\tilde{T}_{\text{BH}}(r) := \frac{1}{\sqrt{2}} \frac{T_{\text{BH}}}{\sqrt{F(r)}} \quad (121)$$

and also defined the degree of freedom of the particle f

$$g_{*f}(T) := \begin{cases} g_f(T) & (f : \text{boson}) \\ \frac{7}{8} g_f(T) & (f : \text{fermion}) \end{cases} \quad (122)$$

for the temperature T with the fermion-correction. The relation (120) is just the thermodynamical relations between the temperature $\tilde{T}_{\text{BH}}(r)$ and the energy density $\rho_f(r)$ except for the spherical geometrical factor $(r_{\text{BH}}/r)^2$. Then our evaluation of the differential particle-number-density (62) is consistent with the picture of a heat-bath around a black hole with the local temperature $\tilde{T}(r)$.

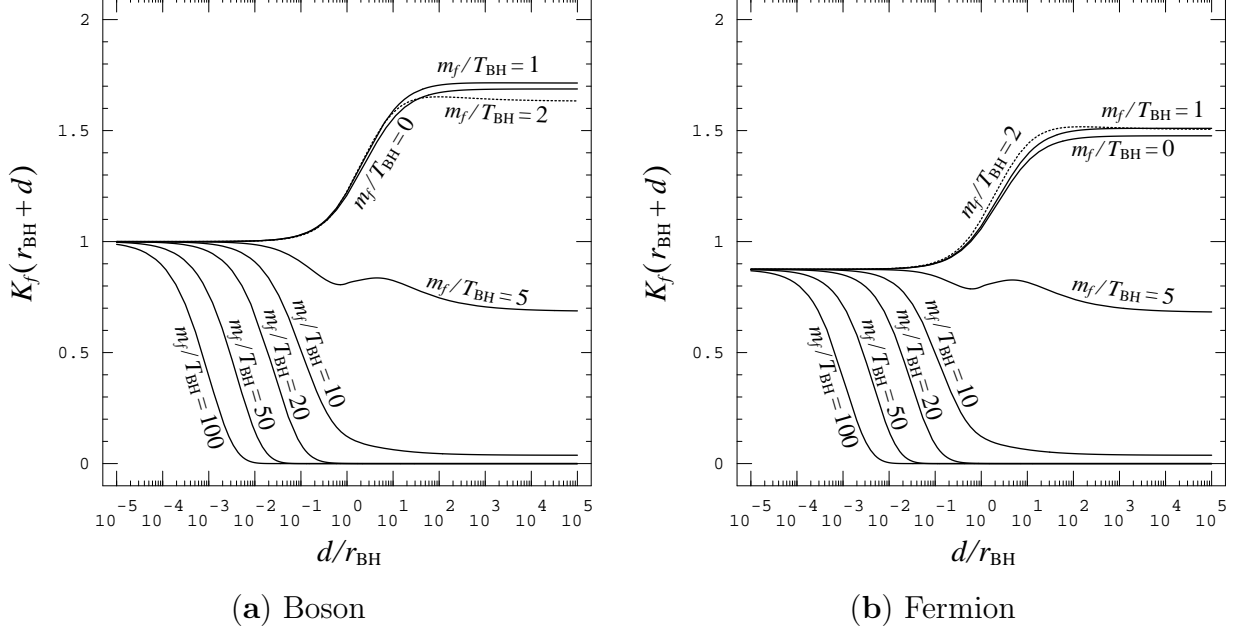


Figure 11: The shapes of the form-function $K_f(\frac{m_f}{T_{\text{BH}}}, r)$ defined in (118) for various m_f/T_{BH} and for (a) bosons and (b) fermions. The horizontal axis d is the distance from the horizon of the black hole with the Schwarzschild radius r_{BH} .

APPENDIX C: Solution near Horizon

We consider the properties of the solution closely near the horizon: $r = r_{\text{BH}} + d$ with $d \ll r_{\text{BH}}$. In the region near the horizon the positive contribution to the Higgs mass term dominates in the effective potential (89) because the Schwarzschild factor $\frac{1}{F(r)}$ becomes very large near the horizon[¶]. The field equation (97) for the profile function $f(s) = \frac{1}{v/\sqrt{2}}\phi(r_{\text{BH}} + d_{\text{DW}}s)$ is approximated to the linear differential equation:

$$\frac{1}{(s_0 + s)} \frac{\partial}{\partial s} \left[(s_0 + s)s \frac{\partial}{\partial s} f \right] = \frac{A^2}{2} \frac{1}{s} f, \quad (123)$$

where we had defined the ratio $s_0 = r_{\text{BH}}/d_{\text{DW}}$. The general solution of this second order differential equation is given by

$$\begin{aligned} f(s) = & C_+ s^{+\sqrt{\frac{A^2}{2}}} \times \\ & {}_2F_1 \left[\frac{1}{2} + \sqrt{\frac{A^2}{2}} - \sqrt{\frac{1}{4} + \frac{A^2}{2}}, \frac{1}{2} + \sqrt{\frac{A^2}{2}} + \sqrt{\frac{1}{4} + \frac{A^2}{2}}, 1 + 2\sqrt{\frac{A^2}{2}}, -\frac{s}{s_0} \right] \\ & + C_- s^{-\sqrt{\frac{A^2}{2}}} \times \\ & {}_2F_1 \left[\frac{1}{2} - \sqrt{\frac{A^2}{2}} - \sqrt{\frac{1}{4} + \frac{A^2}{2}}, \frac{1}{2} - \sqrt{\frac{A^2}{2}} + \sqrt{\frac{1}{4} + \frac{A^2}{2}}, 1 - 2\sqrt{\frac{A^2}{2}}, -\frac{s}{s_0} \right], \quad (124) \end{aligned}$$

[¶]The reason can be regard that the local Hawking temperature $T_{\text{BH}}/\sqrt{F(r)}$ becomes very large.

where ${}_2F_1$ is the hypergeometric function. The coefficients C_+ and C_- are determined by the boundary conditions. The first term is a monochromatic increasing function and has zero value on the horizon ($s = 0$). The second term has singularity on the horizon. To obtain the Higgs vev by the differential equation (123) we have required the boundary conditions; (a) $f(s) \rightarrow 1$ for $s \rightarrow \infty$ and (b) $f(s)$ is finite for $s \rightarrow 0$. Due to the boundary condition (b) the second coefficient C_- should be zero. The first coefficient C_+ is determined by the matching of the solution (124) with $C_- = 0$ and the numerical solution which satisfies the boundary condition (a). As a result of matching to the numerical solutions shown in Figure 9, we obtain $O(1)$ values of C_+ . For example we obtain $C_+ = 0.90$ for $A^2 = 0.001$ with the wall extremely near the horizon, $C_+ = 1.00$ for $A^2 = 0.001$ with $d_{\text{DW}} = r_{\text{BH}}$ and $C_+ = 1.14$ for $A^2 = 0.001$ with larger wall than the scale of the horizon.

The analysis of the Higgs vev near the horizon results that the symmetry broken-down spontaneously by the bare Higgs potential is restored on the horizon $f(0) = 0$ and that the spherical wall-structure of the Higgs vev separates the symmetric phase region on the horizon from the broken phase vacuum in the region distant from the horizon. Therefore the resultant wall-structure is just the “domain wall”, according to the ordinary terminology.

To clarify the behavior of the solution (124), we will consider the extreme cases. When we consider the wall with the near horizon limit, i.e., $s_0 = r_{\text{BH}}/d_{\text{DW}} \rightarrow \infty$, the solution becomes a simple form:

$$f(s) = C_+ s^{+\sqrt{\frac{A^2}{2}}} + C_- s^{-\sqrt{\frac{A^2}{2}}}. \quad (125)$$

When we consider the wall which is extremely distant from the horizon, i.e., $s_0 = r_{\text{BH}}/d_{\text{DW}} \rightarrow 0$, the solution becomes

$$f(s) = C_+ s^{-\frac{1}{2} + \sqrt{\frac{1}{4} + \frac{A^2}{2}}} + C_- s^{-\frac{1}{2} - \sqrt{\frac{1}{4} + \frac{A^2}{2}}}. \quad (126)$$

In both cases, $C_- = 0$ is required by the boundary condition (b). When the wall-formation-constant is much small, i.e., $A^2 \ll 1$, the solution near the horizon which satisfies the boundary condition (b) can be summarized as

$$f(s) \simeq C_+ s^{+\sqrt{\frac{A^2}{2}}}. \quad (127)$$

When we consider the electroweak wall-structure, we have the wall-formation-constant $A^2 \simeq 0.001$ [8] then we can employ this form.

References

- [1] S. W. Hawking, Commun. Math. Phys. **43**, 199 (1975).

- [2] S. W. Hawking, *Nature* **248**, 30 (1974).
- [3] D. B. Cline, *Nucl. Phys. A* **610**, 500C (1996).
- [4] Y. Nagatani, *Phys. Rev. D* **59**, 041301 (1999).
- [5] Y. Nagatani, hep-ph/0104160.
- [6] Y. Nagatani, hep-ph/9805455.
- [7] M. K. Parikh and F. Wilczek, *Phys. Rev. Lett.* **85**, 5042 (2000);
- [8] Y. Nagatani, hep-th/0307294.
- [9] Y. Nagatani, hep-th/0203010.
- [10] J. M. Maldacena and A. Strominger, *Phys. Rev. D* **55**, 861 (1997)
- [11] A. D. Sakharov, *Pisma Zh. Eksp. Teor. Fiz.* **5**, 32 (1967) [*JETP Lett.* **5**, 24 (1967)].
- [12] A. G. Cohen, D. B. Kaplan and A. E. Nelson, *Nucl. Phys.* **B349**, 727 (1991);
- [13] A. G. Cohen, D. B. Kaplan and A. E. Nelson, *Ann. Rev. Nucl. Part. Sci.* **43**, 27 (1993).
- [14] K. Hotta, *Prog. Theor. Phys.* **99**, 427 (1998).